

Polyoxometalates Assemblies and Their Electrochemical Applications

Wenjing Liu, Xiao-Li Wang, and Ya-Qian Lan

Abstract Polyoxometalates (POMs) possess a large structural and compositional variety, coupled with their highly redox activity, leading to applications in deriving advanced materials for clean and renewable energy storage and conversion. The synthetic strategies used to prepare POM-assisted nanocomposites are discussed. The principal classes of POM derived electrocatalysts reported so far, such as polyoxometalates based metal-organic framework (POMOFs) materials, metal carbides, metal oxides, metal sulfides, and heteroatom-doped carbon materials for hydrogen evolution reaction (HER), oxygen evolution reaction (OER), and the overall water splitting are reviewed. These composites provide a chemist's way to prepare highly efficient and low-cost non-noble metal electrocatalysts.

Keywords HER • OER • Overall water splitting • Polyoxometalate

Contents

- 1 Introduction
 - 1.1 General Considerations of Water Splitting
 - 1.2 Advantages of Polyoxometalates for Hydrogen Evolution Reaction and Oxygen Evolution Reaction
 - 1.3 Scope of This Chapter
- 2 Measurement Criteria for Characterizing the Electrochemical Activity
- 3 Synthetic Strategies Used for Constructing Polyoxometalates Based Materials
- 4 Polyoxometalates Based Metal-Organic Framework Materials
 - 4.1 Polyoxometalates Based Metal-Organic Framework Single Crystal Materials
 - 4.2 Polyoxometalates Based Metal-Organic Framework-Based Composites as Electrocatalysts

1 Introduction

The development of clean and efficient new energy has attracted great research interest in recent years because of fast exhaustion of fossil fuels, environmental contamination, greenhouse effect, etc. The preparation of clean energy by electrolyzing water is an efficient and effective alternative to fossil fuels [1]. Electrochemical energy conversion systems including chlor-alkali electrolyzer [2], water-alkali electrolyzer [3], metal-air batteries [4–8], solar water-splitting devices [9, 10], artificial leaves [11], and proton exchange membrane electrolyzer [12–15] are expected to produce contemporary clean energy. However, in the practical application, their performance is hindered by high activation barriers, leading to large overpotentials [16]. It is thus attractive to develop active, cost-effective, and earth-abundant electrocatalysts for the water electrolysis industry that can be commercialized at a large scale. Progress has been made in recent years in designing such active electrocatalysts including metal carbide (e.g., Mo_2C , W_2C) [17–20], metal nitrides (e.g., MoN) [21–24], metal oxide (e.g., CoO , Co_3O_4 , and MoO_2), metal sulfide (e.g., MoS_2 , WS_2 , CoS_2 , and VS_2) [25–30], metal phosphide (e.g., MoP , Ni_2P , FeP , and CoMoP) [31–35], metal layered double hydroxides (e.g., NiFe LDH, NiV LDH) [36–39], heteroatom-doped carbon (e.g., N,P-codoped nanocarbon) [40–43], etc.

1.1 General Considerations of Water Splitting

As shown in Fig. 1, an electrolyzer in which the overall water-splitting reaction happens can be divided into two-half reactions: the hydrogen evolution reaction (HER) of the cathode and the oxygen evolution reaction (OER) of the anode. When an external voltage is applied to the electrodes, water molecules are electrolyzed into hydrogen occurring in HER and oxygen accompanied with OER. According to the electrolytes with various pHs in which water splitting carries out, the water splitting can be described as follows:

The whole reaction:

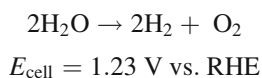
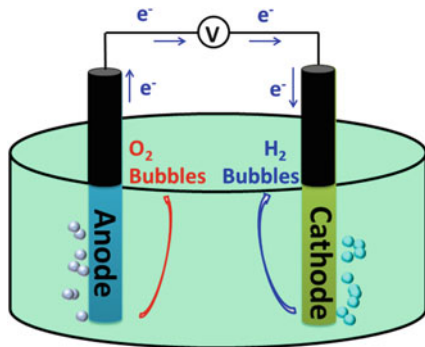
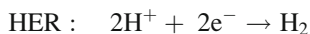
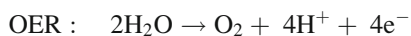


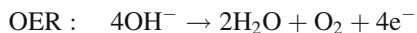
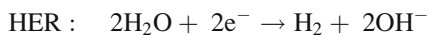
Fig. 1 Schematic diagram illustrating the two-electrode water electrolyzer



In acidic media,



In neutral or alkaline media,



The theoretical minimum voltage required for the electrochemical water splitting is 1.23 V at 25°C regardless of the electrolytes in which water splitting takes place. The practical operational voltage is larger than the theoretical potential due to the existence of the resistances which would consume lots of electricity. Thus, the applied voltage for water splitting can be described as [44, 45]:

$$E_a = 1.23 \text{ V} + \eta,$$

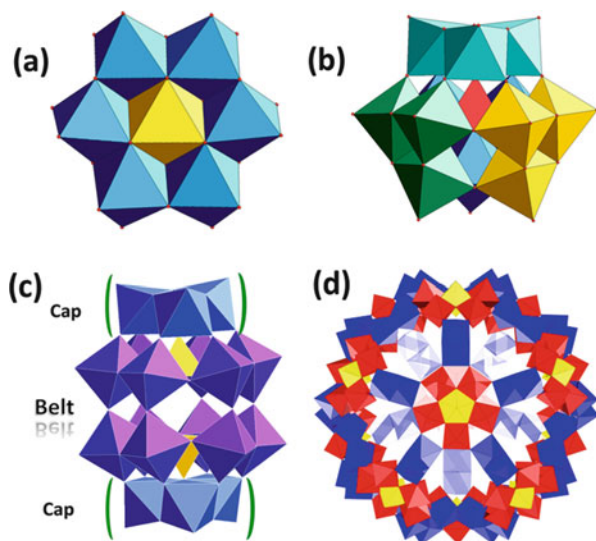
where η includes the overpotentials desired for overcoming intrinsic activation obstacles of both anode and cathode, and the external potentials required for compensating the systematic resistances, e.g., electrolyte resistance and contact resistance. From this point of view, highly active electrocatalysts are desirable in water electrolyzers if they could reduce the overpotential and improve the efficiency of water electrolysis.

1.2 Advantages of Polyoxometalates for Hydrogen Evolution Reaction and Oxygen Evolution Reaction

Polyoxometalates (abbreviated POMs), as its name suggests, represent a class of multi-metal oxyanions usually formed by early transition metals pertaining a d^0 or d^1 electron configuration (e.g., V^V , Mo^V , Nb^V , Ta^V , Mo^{VI} , and W^{VI}). According to this definition, we can use a general formula $[M_mO_y]^{p-}$ to describe them, where M can be visualized as the central metal of a polyhedron, and O can be regarded as the vertices of that polyhedron. These polyhedra can be connected to each other via corner- or edge-sharing modes (face sharing is rarely seen). These structural building blocks may be used to prepare or conceptualize the primary, secondary, and tertiary structures of the POM clusters [46]. Therefore, the different structural POM assemblies can be formed by the linking or aggregation of these polyhedra via a self-assembly process. POM chemistry has developed exponentially due to the modern instrumentation and novel synthetic approaches, starting from the 1991 review [47]. The development of single crystal X-ray diffraction technique has allowed collecting the diffraction data to obtain the aesthetically beautiful structure and the availability of multinuclear NMR spectroscopy has led to a clearer understanding of the structure solution chemistry. The most common and widely studied POMs with dimensions of ca. 1–6 nm are as follows: (a) The Anderson-Evans $[XM_6O_{24}]^{n-}$ is a planar arrangement of six MO_6 octahedra with a central heteroatom XO_6 octahedron, resulting in an overall D_{3h} -symmetric shape (Fig. 2a) [48–50]. (b) The Keggin $[XM_{12}O_{40}]^{n-}$ is composed of a central XO_4 tetrahedron surrounded by four corner-shared $\{M_3O_{13}\}$ groups with each triad being composed of three edge-shared MO_6 octahedra, resulting in an overall T_d -symmetry (Fig. 2b) [51]. (c) The Wells-Dawson $[(XO_4)_2M_{18}O_{54}]^{n-}$ is assembled by the fusion of two trlacunary Keggin-type units $[XM_9O_{34}]^{n-}$ via corner sharing at the vacant sites. This structure consists of two unequivalent metal centers, the caps (polar positions) and belts (equatorial regions), where the cap is composed of three edge-shared MO_6 octahedra forming an $\{M_3O_{13}\}$ triad and the belt is formed by alternating corner- and edge-shared MO_6 octahedra, as shown in Fig. 2c [52]. (d) The famous Kelperate structure $[Mo_{72}^{VI}Mo_{60}^VO_{372}(CH_3COO)_{30}(H_2O)_{72}]^{42-}$ could be abbreviated as $\{Mo_{11}\}_{12}$ with remarkable equivalent stoichiometrical building blocks. The Keggin $\{Mo_{11}\}$ is composed of a central $\{(Mo)^{VI}Mo_5^{VI}\}$ pentagonal bipyramid surrounded by five $\{Mo_1^V\}$ as linkers [53]. Müller pioneered the study of Kelperate spherical POMs (Fig. 2d).

One of the most striking features of POMs is that they could configure and tailor their redox characteristics, reversibly gain and lose up to 24 electrons per unit for the Keggin ion $[PMo_{12}O_{40}]^{3-}$. This phenomenon has been verified by in operando X-ray absorption studies [54]. POMs, structurally well-defined molecular species, together with their unique redox properties, have led to a myriad of applications in electrocatalysis [51, 55–58], electronic and energy storage devices [59], magnetic science [60], as well as in analytical and clinical chemistry including spectroscopy [61], biology [62–64], and catalysis [65–69].

Fig. 2 Polyhedral representations of polyoxometalate (POM) anions, highlighting their structural variety. (a) Anderson anion; (b) Keggin anion; (c) Dawson anion; and (d) $\{\text{Mo}_{132}\}$ ball shaped cluster



1.3 Scope of This Chapter

Though vast breakthroughs had been achieved in designing and applying POM-based composites [70–73], it was not until the contemporary time that scientific communities have paid attention to their potentials in the field of electrochemical catalysis. In this chapter, we will briefly introduce the principle of water electrolysis and the regular parameters for the determination of the catalytic activity. Then, we will give an overview of the principal synthetic strategy for POM-based composites including polyoxometalates based metal-organic frameworks (POMOFs), and POMs encapsulated in nanocarbon materials. Meanwhile, we will systematically summarize the performance of POM-based composites. More importantly, we expect that this chapter could provide guidance to rational design and controllable syntheses of POM-based electrocatalysts, which are useful for the further applications in mediators for electrochemical water splitting.

2 Measurement Criteria for Characterizing the Electrochemical Activity

To evaluate the performance of electrocatalysts fairly, the kinetic parameters such as overpotential (η), exchange current density (j_0) and Tafel slope (b) are required to be measured or calculated carefully. The overpotential (η) is one of the most important benchmarks to elucidate the catalytic activity of the target electrocatalysts. It is generally logarithmically related to the current density (j) as given by Tafel equation: $\eta = a + b \log(j)$. The exchange current density (j_0) is

yielded when this linear relationship η is extrapolated to be zero, describing the intrinsic activity of the electrode under equilibrium conditions [74]. The desirable electrocatalysts should possess a high exchange current density (j_0) and a low Tafel slope (b) in order to be useful at the applied current densities. In practice, the most convenient way to determine the electrocatalytic ability for the target reaction is stating the overpotential at a current density of 10 mA cm^{-2} . Here, precautions have to be taken because different current densities are referred to different overpotential. Therefore, the current density of the reported overpotential should be stated.

Apart from the above discussed parameters used for developing excellent electrocatalysts, some other factors for designing catalytic materials are also very important. The construction of an ideal electrocatalyst should be considered in the light of the following three principles: (1) high activity; the more active sites (the part where catalysis reaction can happen) that the catalysts have, the better they are for evolution reactions. (2) Long-term stability; the continuous hydrogen evolution or oxygen evolution could last for over 8 h while the catalyst activity would not be reduced. There are two approaches for characterizing its stability. One way is to measure the current variation with time ($I-t$ curve). The other method is to conduct the cycling experiment by using linear sweep voltammetry (LSV) and cyclic voltammetry (CV). More precisely, if the number of cycles is over 5,000, it indicates that the material has good stability [44]. (3) High selectivity; the Faraday efficiency of the reaction process is calculated by comparing the ratio of the experimentally detected hydrogen or oxygen amount to the theoretically calculated hydrogen or oxygen amount, which should be close to 100%. Currently, industrial electrolytic water catalysts include commercially available Pt/C electrocatalysts for HER and IrO_2 or RuO_2 catalysts for OER. These two types of precious metals are the most important benchmarks to determine the performance of the catalysts. However, the noble metals are exorbitantly costly. There is an urgent need to develop highly efficient, cost-effective, and earth-abundant non-precious metal catalysts.

3 Synthetic Strategies Used for Constructing Polyoxometalates Based Materials

Due to the rich composition of the high oxidation states of V, Mo, and W (V^{V} , Mo^{VI} , and W^{VI}), POMs are supposed to be a perfect candidate to prepare high efficient electrocatalysts. Cronin et al. have introduced the concept of electron-coupled-proton buffer (ECPB), whereby the OER was decoupled from the HER, O_2 and H_2 can be produced separately in both space and time [75]. It broke through the conventional water electrolysis producing H_2 and O_2 simultaneously, but the catalysis of $\{\text{PMo}_{12}\}$ was weak. Moreover, it had high requirement regarding the catalysts, e.g., they should have reversible redox waves between OER and HER, should be highly soluble in

water, and should effectively buffer the pH variations without any degradation during the water-splitting process. Indeed, most of POMs as electron and proton reservoir could undergo reversible multi-electron processes in the homogeneous liquid media. However, their applications as very efficient heterogeneous electrocatalysts are circumvented by the following drawbacks: (1) they are very soluble in water or electrolyte, which is not good for isolating and recycling them from the solution; and (2) they have low specific surface area ($<10 \text{ m}^2 \text{ g}^{-1}$), which are not conducive to catalytic performance.

There are two synthetic strategies here for solving this problem. One method is to immobilize POMs in porous metal-organic framework (MOF). MOFs represent a branch of porous materials with high surface area, highly ordered permanent porosity, and tunable chemical structures, and they are excellent candidates for carriers. Because POMs are either as a template occupied in the cavities of MOFs or directly part of the frameworks of MOFs, such kinds of materials are termed as POMOFs materials. The other method is to load POMs evenly between graphene oxide (GO) or some other carbon materials. Furthermore, GO-based materials are nontoxic, chemically tolerant, which is possible to be exfoliated into single layers as carrier uniformly in aqueous solution. Because of the insolubility of the POMOFs and POM-based carbon materials, the electrochemistry of the composites is allowed to be performed in the solid state by entrapping them in a perfluorinated polymer (Nafion). Those composites are anticipated to be useful for efficient electrocatalysts elaboration. Furthermore, on theoretical grounds, the entrapment of POMs in a 3D configuration could increase their electrocatalytic activity [56, 76]. Those strategies Su and Lan adopted here offer an effective and feasible way for preparing electrocatalytic materials with low solubility and high surface area.

4 Polyoxometalates Based Metal-Organic Framework Materials

4.1 Polyoxometalates Based Metal-Organic Framework Single Crystal Materials

Hybrid materials involving the combination of metal-organic complexes and POMs have been met in the past few decades. There are essentially two key factors, stability and porosity, utilizing POMOF as electrocatalysts. Compared with the traditional MOFs, though vast examples of POMOFs have been usually synthesized in water with good stability, the porosity of the synthesized single crystals is small due to the lack of organic solvent as template during the synthetic process. It is natural to ask the question: how to synthesize porous and stable POMOFs? According to the structural diversity, POMOFs could be classified into three categories: (1) POMs serving as nodes connected with the rigid ligand, (2) POMs

serving as a template encapsulated within the cavities of MOFs, and (3) POMs anions serving as pillars. As shown in Fig. 3, the second one and the third one are easier to support the channel compared to the first one where the cavities of the resulting porous materials are partially occupied. Therefore, researchers draw this idea to design POMOFs. Then, a new synthetic challenge came: how do the anionic POMs coordinate to organic ligands?

POMOFs are usually prepared by utilizing POMs precursors, organic ligands, and metal ions via conventional bottom-up aqueous solution methods or hydro-/solvo-/iono-thermal methods [77]. Although POMOFs-based materials have been studied extensively as catalysts [77–79], there were only a few reports on POMOFs utilized as electrocatalysts [80]. Dolbecq et al. primarily studied the cation effect on the electrocatalytic activities of $(\text{TBA})_3[\text{PMo}^{\text{V}}_8\text{Mo}^{\text{VI}}_4\text{O}_{36}(\text{OH})_4\text{Zn}_4][\text{C}_6\text{H}_3(\text{COO})_3]_{4/3} \cdot 6\text{H}_2\text{O}$ ($\epsilon(\text{trim})_{4/3}$, TBA^+ = tetrabutylammonium ion) in XCl ($\text{X} = \text{Li}, \text{Na}, \text{K}, \text{Cs}$) media [80]. The material represented the first example of non-noble POM-based materials and showed a turnover frequency (TOF) as high as ca. 6.7 s^{-1} with $\eta = 200 \text{ mV}$ for HER. Dolbecq et al. synthesized five compounds. These compounds all contain $\{\text{Zn}-\epsilon\text{-Keggin}\}$ fragments and organic ligands, in which $\{\text{C}_6\text{H}_3(\text{COO})_3\}$ of $\epsilon(\text{trim})_{4/3}$ was substituted by some other types of organic

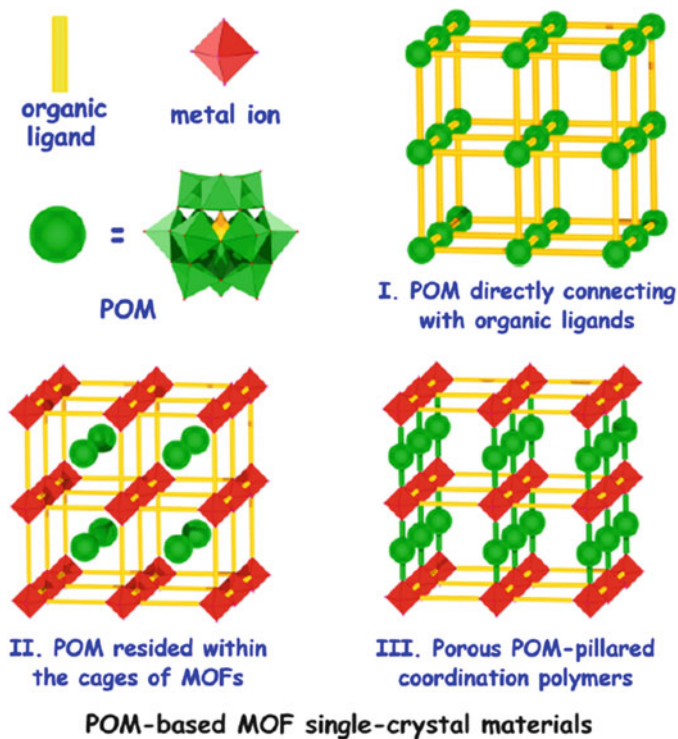


Fig. 3 Schematic views of three main forms of polyoxometalates based metal-organic framework (POMOFs) materials. Reprinted with permission [77]. Copyright 2014, Royal Society of Chemistry

linkers. Those hybrids also showed remarkable behaviors for HER which is mainly due to the presence of $\{\text{Zn-}\epsilon\text{-Keggin}\}$ units as well as their special structures.

Lan's group modified the Keggin type of $\{\text{PMo}_{12}\}$ through the decoration of transition metal to synthesize the coordinated chloride ion and zinc modified Zn- ϵ -Keggin-Cl (**NENU-499**, $(\text{TBA})_4[\epsilon\text{-PMo}^{\text{V}}_8\text{Mo}^{\text{VI}}_4\text{O}_{37}(\text{OH})_3\text{Zn}_4]\text{Cl}_4$). After that, chloride ions were substituted by the carboxylate group. Density functional calculations showed that the binding energy value of POMs coordinated chloride ions was smaller than that of carboxylate group and demonstrated that POMs with carboxylate groups were more stable than those with chloride ions. This provided a theoretical basis for the next step in the construction of porous POMOFs (Fig. 4).

In view of the above discussed strategies, $\{\text{Zn-}\epsilon\text{-keggin}\}$ fragments [81] serving as nodes were linked to ligands with different sizes, respectively, to form POMOFs with different frameworks, $\epsilon(\text{trim})_{4/3}$ [80], $(\text{TBA})_3[\epsilon\text{-PMo}^{\text{V}}_8\text{Mo}^{\text{VI}}_4\text{O}_{36}(\text{OH})_4\text{Zn}_4]$ [BTB] $_{4/3}\cdot x\text{Guest}$ (**NENU-500**, BTB = benzene tribenzoate) [81], and $(\text{TBA})_3[\epsilon\text{-PMo}^{\text{V}}_8\text{Mo}^{\text{VI}}_4\text{O}_{36}(\text{OH})_4\text{Zn}_4][\text{BPT}]_{4/3}\cdot x\text{Guest}$ (**NENU-501**, BPT = (1,1'-biphenyl)-3,4',5-tricarboxylate) [81] (Fig. 5). The N_2 adsorption curve showed that the crystal structure changes from nonporous to microporous as the rigidity of the ligand increases. Powder X-ray diffraction (PXRD) of the compounds under different pH values showed that they had good chemical stability. As an electrochemical hydrogen evolution catalyst, porous POMOF **NENU-500** had the best electrochemical activity compared to other MOFs and POMOFs (**NENU-501**, $\epsilon(\text{trim})_{4/3}$,

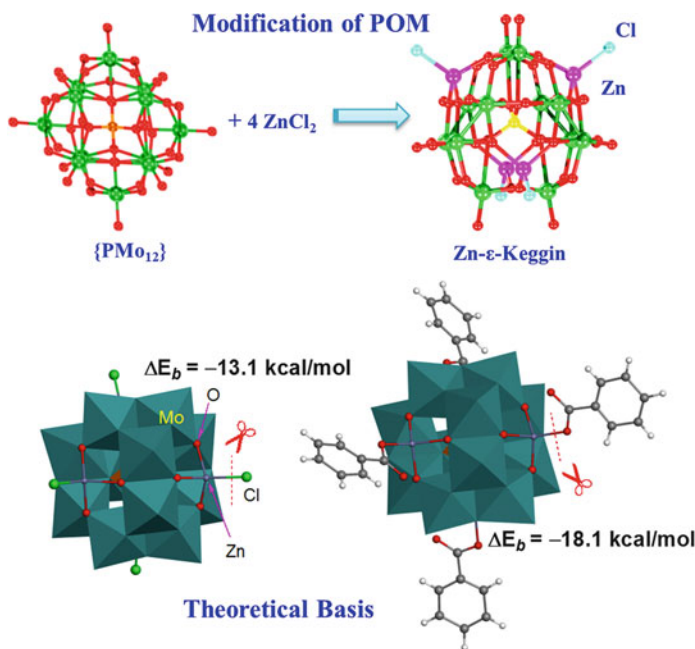


Fig. 4 Theoretical basis of designing POMOFs. Reprinted with permission [81]. Copyright 2015, American Chemical Society

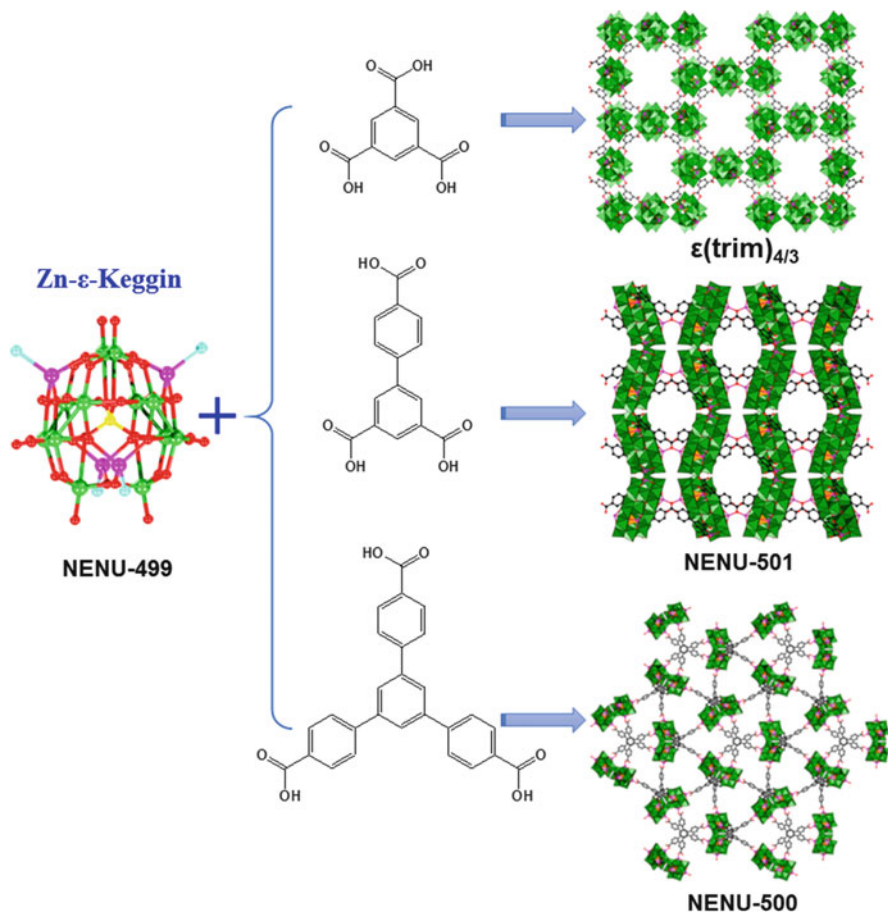


Fig. 5 Schematic views of three types of POMOFs single crystal materials with different sizes of pores

NENU-499, **NENU-5**, and **HKUST-1**) due to its good stability, highly porosity, and exposed active sites. It showed an onset potential of 180 mV and an overpotential of 237 mV at the current density of 10 mA cm^{-2} (Fig. 6a). The performance comparison showed that the extensive porosity has a great influence on the electrochemical activity of POMOFs. Tafel slope is also a very important parameter for evaluating an inherent property of electrocatalytic materials and elucidating HER mechanism involved. Figure 6b displayed the Tafel plots for the corresponding materials. The Tafel slopes of commercially available Pt/C, **NENU-500**, **NENU-501**, $\epsilon(\text{trim})_{4/3}$, **NENU-499**, **NENU-5**, and **HKUST-1** obtained from the Tafel plots are 30, 96, 137, 142, 122, 94, and 127 mV dec^{-1} , respectively. In summary, POMOFs single crystal materials are successful examples that POMs could be immobilized in MOFs evenly at the atomic or molecular level. This unique feature of POMOFs combining the redox activity of POMs and the porosity of MOFs opens up a new path for designing more efficient catalysts.

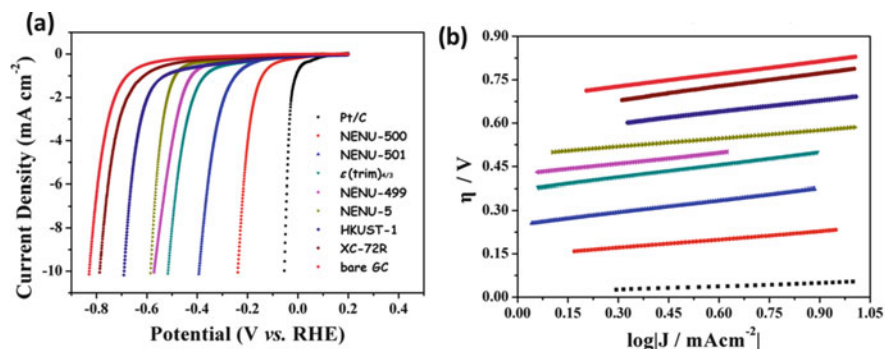


Fig. 6 (a) Hydrogen evolution reaction (HER) polarization curves of various electrocatalysts in 0.5 M H₂SO₄ aqueous solution. (b) Tafel plots of the corresponding catalysts. Reprinted with permission [81]. Copyright 2015, American Chemical Society

4.2 Polyoxometalates Based Metal-Organic Framework-Based Composites as Electrocatalysts

POMOFs have the advantage of POMs (redox activity) and the advantage of MOFs (porosity). Hence, they form appealing structures and show potential applications. Moreover, due to the inherent presence of Mo, P, and N-moieties in POMOF structures, the POMOFs present ideal sacrificial precursors to derive bimetallic composite electrode materials. The research of POMOFs has been extended from single crystal synthesis to material application. POMOFs as the precursors to prepare the electrochemically active carbon-based composite provide a new idea for the synthesis of the electrocatalysts. Lou et al. prepared porous molybdenum carbide octahedral nanoparticles (MoC_x nano-octahedrons) starting from NENU-5 in situ carburization reaction as a proof of concept exhibiting remarkable electrocatalytic performance for HER in both acidic and basic solutions with good stability (Fig. 7) [82]. It showed an onset potential of 25 mV, an overpotential of 142 mV at the current density of 10 mA cm⁻², and a small Tafel slope of 53 mV dec⁻¹ in acidic condition. The HER performance in basic solution was also favorable with an onset potential of 80 mV, an overpotential of 151 mV at the current density of 10 mA cm⁻², and a small Tafel slope of 59 mV dec⁻¹ (Fig. 8).

The study on POMOFs-based catalysts has been further extended to explore porous heteroatom-doped carbon hybrids because the dopant of heteroatoms has the advantage of offering more active sites to enhance their catalytic performance. Lan et al. synthesized the Fe₃C/Mo₂C-containing N,P-codoped graphitic carbon derived from POM@MOF-100 (Fe) (denoted as Fe₃C/Mo₂C@NPGC) catalyst by carbonizing the mixture of PMo₁₂@MIL-100 (Fe) and melamine at 900°C in a flow of ultrapure N₂ atmosphere (Fig. 9) [83]. By the ingenious synthetic strategy “killing three birds with one stone” the author adopted here, the as-synthesized catalyst had the characteristics of uniform distribution, mesoporous structures, and N, P-heteroatom codoped graphitic carbon. The contradistinctive catalysts Fe₃C@C

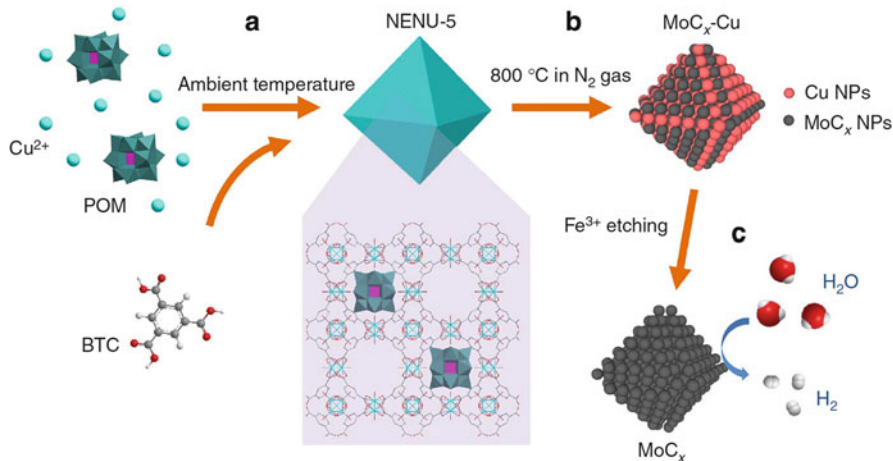


Fig. 7 Preparation processes of porous MoC_x nano-octahedrons. (a) Synthesis of NENU-5 nano-octahedrons with $\{\text{PMo}_{12}\}$ residing in the pores of HKUST-1 host. (b) Formation of $\text{MoC}_x\text{-Cu}$ nano-octahedrons after carburization reaction. (c) Removal of Cu nanoparticles by Fe^{3+} etching to prepare porous MoC_x nano-octahedrons for HER [82]. Copyright 2015, Nature Publishing group

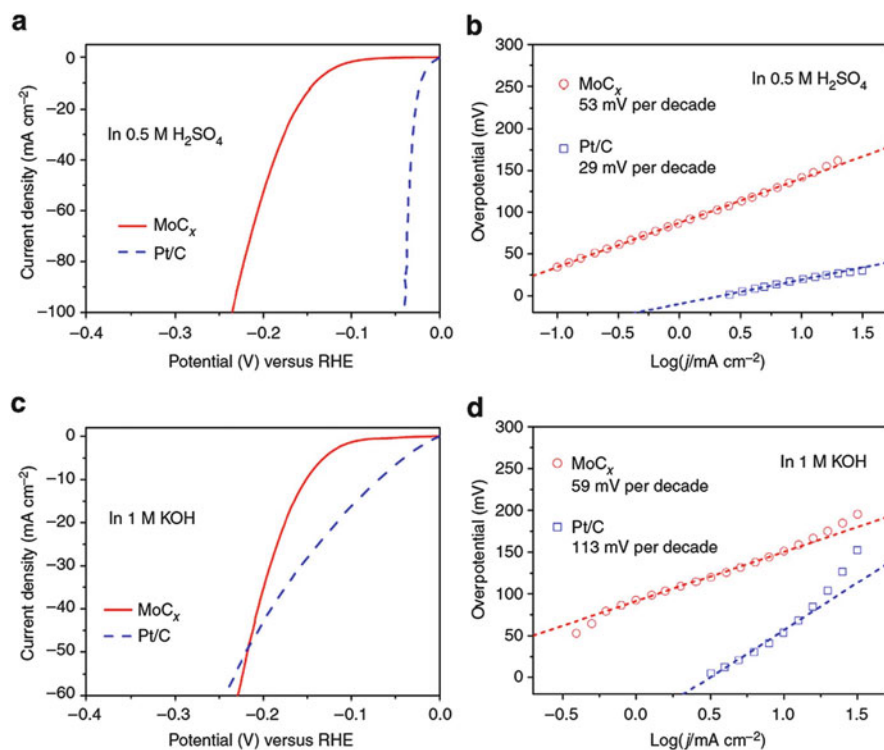


Fig. 8 (a) Polarization curves at 2 mV s^{-1} of porous MoC_x nano-octahedrons and Pt/C in $0.5\text{ M H}_2\text{SO}_4$ solution. (b) Tafel plots in $0.5\text{ M H}_2\text{SO}_4$. (c) Polarization curves at 2 mV s^{-1} in 1 M KOH . (d) Tafel plots in 1 M KOH [82]. Copyright 2015, Nature Publishing group

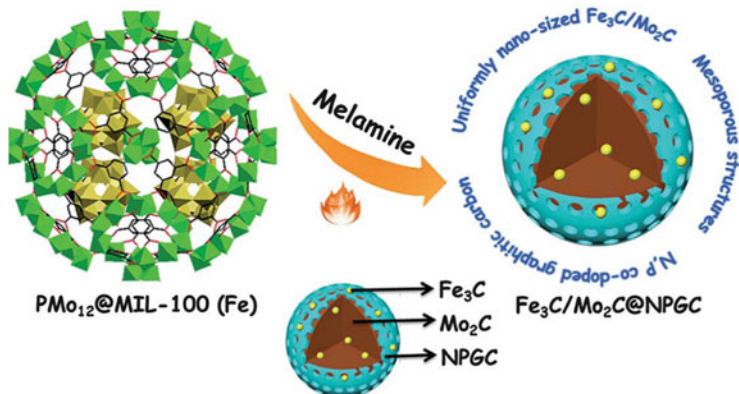


Fig. 9 Preparation process of the $\text{Fe}_3\text{C}/\text{Mo}_2\text{C}@\text{NPGC}$ nanocomposite. Reproduced from [83] with permission from The Royal Society of Chemistry

and $\text{Fe}_3\text{C}/\text{FeMo}/\text{Mo}_2\text{C}$ were also synthesized via the carbonization of the pure MIL-100 (Fe) or $\text{PMo}_{12}@\text{MIL}-100$ (Fe) under the same conditions, respectively (Fig. 10). The material $\text{Fe}_3\text{C}/\text{Mo}_2\text{C}@\text{NPGC}$ exhibited high HER activity with a low onset potential of 18 mV (vs. RHE), an overpotential of 98 mV at the current density of 10 mA cm^{-2} , a small Tafel slope of 45.2 mV dec^{-1} as well as long-term durability for 10 h.

The noble metal-free HER catalysts still could not replace the Pt or Pt-based nanomaterials because the performances of POMOFs-based catalysts are worse than Pt-group metals. Then, Lan's group have fabricated a hybrid material consisting of MoO_2 , phosphorus-doped nanoporous carbon, and reduced graphene oxide (RGO) substrates (denoted as $\text{MoO}_2@\text{PC-RGO}$, Fig. 11) by using a POMOFs/GO-assisted strategy for the following considerations: First, $\{\text{PMo}_{12}\}$ is rich in molybdenum and phosphorus moieties [84]. Second, graphene sheets as support have been introduced into POMOFs for electrocatalysts, which are one of the most promising components because of their characteristics of large surface area, chemical toleration, good conductivity, and high stability [85]. Third, the agglomeration of MoO_2 can be hindered by confining the carbon skeleton, and $\text{MoO}_2@\text{PC}$ hybrids are loaded onto RGO evenly because of the defined and distinct structure of the POMOFs/GO composite. Phosphorus is doped with $\text{MoO}_2@\text{PC-RGO}$ through P–C and P–O bonds and it offers the active sites for catalysts. The nanosized POMOF/GO composites were prepared first by utilizing the NENU-5 as precursors and GO. The final product was successfully synthesized by carbonizing the mixture of POMOF/GO composites at 800°C in a flow of ultrapure N_2 atmosphere and successively by acid-leaching with 3 M HCl. We have to mention that the calcination duration played a key role in obtaining the final product because MoO_2 species were reduced to MoC_2 upon increasing the carbonizing time to 5 h. The $\text{MoO}_2@\text{PC-RGO}$ nanocomposite exhibited an excellent HER electrochemical activity in acidic solution, with the onset potential close to 0 mV, approaching that

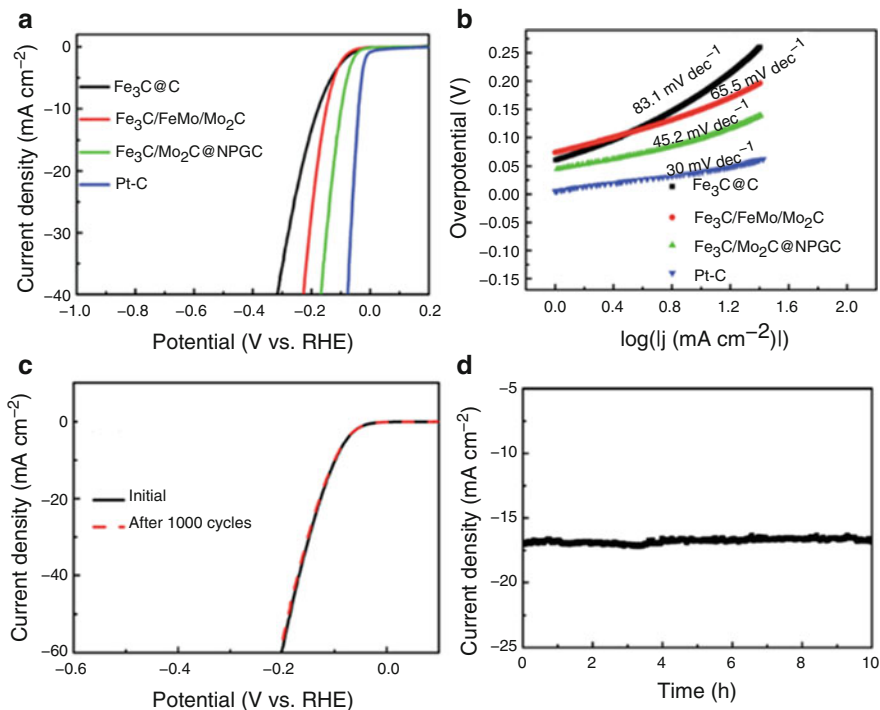


Fig. 10 (a) Polarization curves of different samples. (b) Corresponding Tafel plots of the polarization curves. (c) Polarization curves of $\text{Fe}_3\text{C}/\text{Mo}_2\text{C}@NPGC$ initially and after 1,000 cycles. (d) Time dependence of current density under a static overpotential of 120 mV for 10 h. Reproduced from [83] with permission from The Royal Society of Chemistry

of commercially available Pt/C, an overpotential of 38 mV at the current density of 10 mA cm^{-2} , a small Tafel slope of 41 mV dec^{-1} as well as remarkable long-term cycle stability (Fig. 12).

Li et al. also devoted efforts on exploring non-noble metal substitutes derived from POMs precursors instead of Pt-based electrocatalysts [86]. The molybdenum carbide nanoparticles $\text{MoC}_x@C-1$ and MoC_x-2 were prepared from the starting two types of POMOFs as precursors which were further carbonized at 800°C in a flow of ultrapure N_2 atmosphere and acid-leached with 1 M HCl so as to remove the inactive metallic metal (Fig. 13). The measurements showed that the $\text{MoC}_x@C-1$ with N dopants and graphene coatings were superior to that of uncoated MoC_x-2 nanoparticles. $\text{MoC}_x@C-1$ exhibited a low onset potential of 21 mV and an overpotential of 79 mV at the current density of 10 mA cm^{-2} , a small Tafel slope of 56 mV dec^{-1} as well as remarkable long-term cycle stability (Fig. 14). Hence, the confined carburization strategy by using POMOFs as precursors is an extremely promising method for synthesizing other non-noble metal oxides or carbides confined carbon skeletons used as electrocatalysts for water splitting.

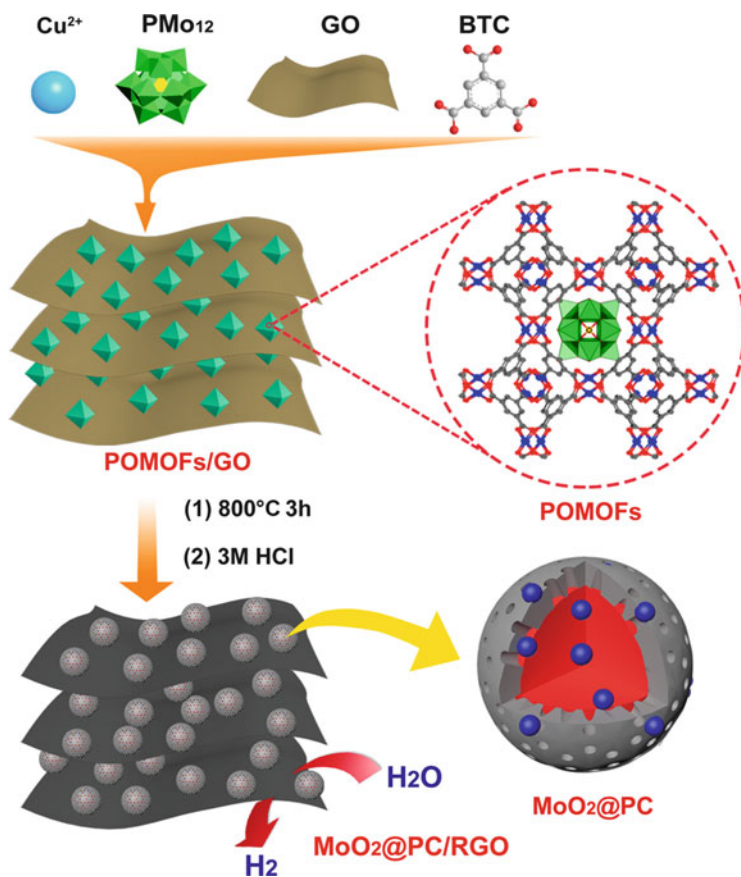


Fig. 11 Schematic construction of the $\text{MoO}_2\text{@PC-RGO}$ nanocomposite. Copyright 2015, [84] Wiley

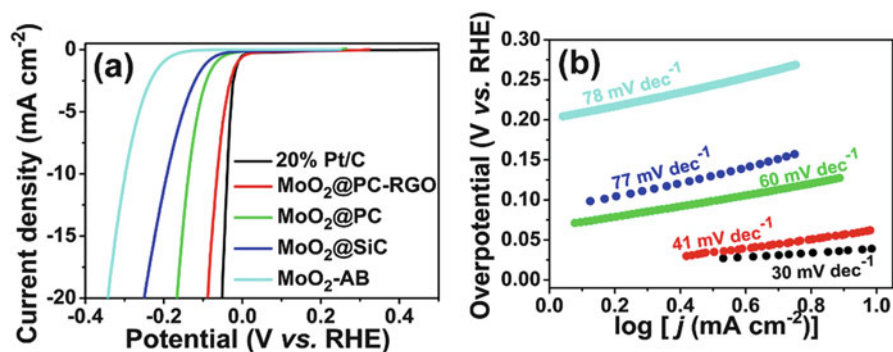


Fig. 12 (a) Polarization curves for four electrocatalysts and 20% Pt/C. (b) Tafel plots of the corresponding polarization curves. Copyright 2015, [84] Wiley

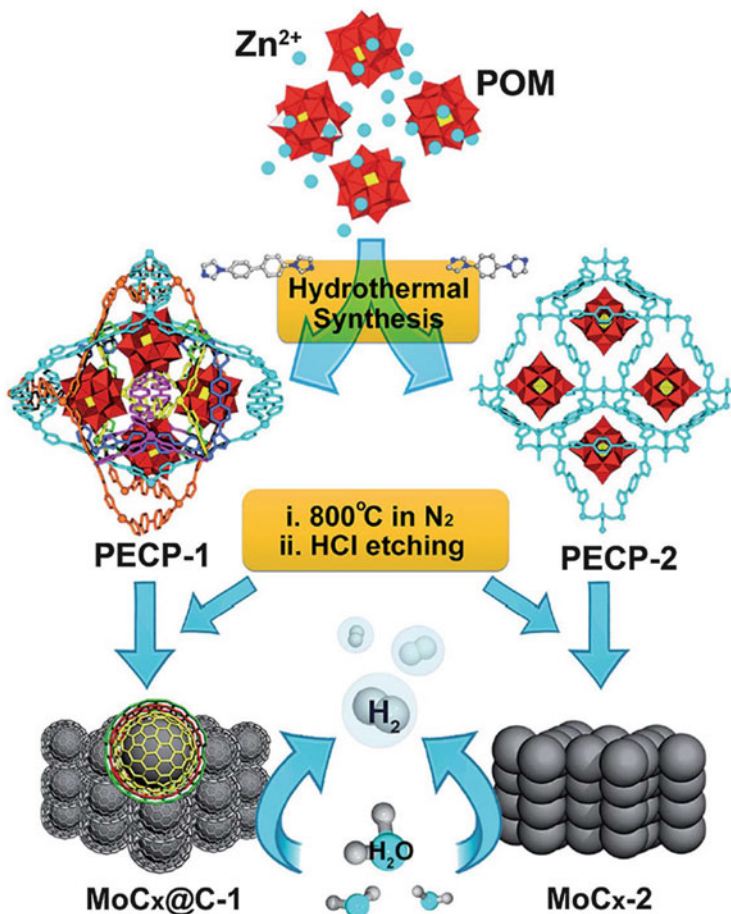


Fig. 13 Schematic constructions of molybdenum carbide nanoparticles [86]. Copyright 2016, Royal Society of Chemistry

5 Polyoxometalate–Carbon Composites

The attachment of POMs in a 3D configuration could boost their electrocatalytic activity. This trend was termed as “microenvironment effect.” It was verified not only by theory but also by experiment evidence. Take several effective POM-based electrocatalysts, for example, Korts’s polyanions, $[\text{Cu}^{\text{II}}_2\text{Pd}^{\text{II}}_{22}\text{P}^{\text{V}}_{12}\text{O}_{60}(\text{OH})_8]^{20-}$ [87], $[\text{Co}_6(\text{H}_2\text{O})_{30}\{\text{Co}_9\text{Cl}_2(\text{OH})_3(\text{H}_2\text{O})_9(\beta\text{-SiW}_8\text{O}_{31})_3\}]^{5-}$, $[\{\text{Co}_3(\beta\text{-}\beta\text{-SiW}_9\text{O}_{33}(\text{OH}))(B\text{-}\beta\text{-SiW}_8\text{O}_{29}\text{OH})_2\}]^{22-}$ [56], which were fixed on the low-cost carbon material Vulcan XC-72 for the HER in acidic aqueous solutions; $\{\text{Co}_7(\text{AlePy})_2\}$, which was immobilized on Vulcan XC-72 for oxygen reduction reactions in basic aqueous solutions with superior durability than that of commercially available Pt/C [88]. As we all know, atom doping has great effect on HER performance because of electronic

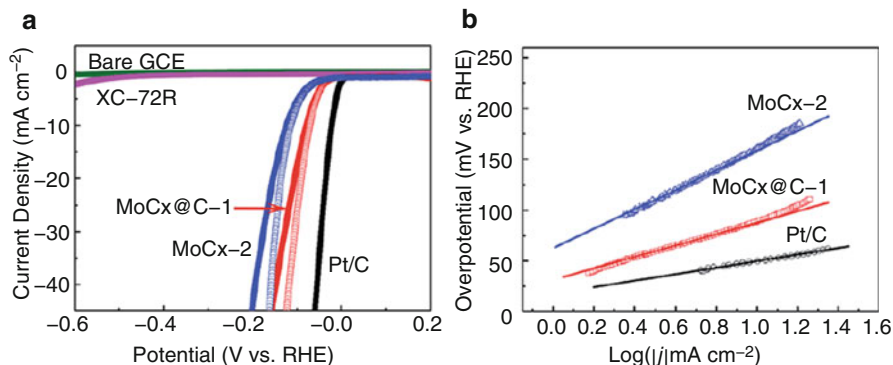


Fig. 14 Electrochemical characterization of the prepared catalysts: (a) polarization curves of MoC_x@C-1, MoC_x-2, 20%Pt/C, and pure carbon black (XC-72R). (b) Tafel plots of the corresponding composites [86]. Copyright 2016, Royal Society of Chemistry

structural modification [89]. Wang et al. reported 3D urchin-like Mo doping-W₁₈O₄₉ nanocomposite as an efficient HER catalysts with an onset potential of 23 mV, an overpotential of 40 mV at the current density of 10 mA cm⁻², a small Tafel slope of 54 mV dec⁻¹ as well as long-term durability [90]. Density functional theory calculations revealed that such impressive HER performance is due to the existence of Mo dopant to increase the number of active sites, leading to optimal hydrogen adsorption on the active sites because of the electronic and geometric modulation. In addition, carbon nanotubes (CNTs) have the particularities of hollow geometry, high surface area, and high electronic conductivity. Xu et al. reported a hybrid based on CNTs and the classical 12-tungstophosphate [PW₁₂O₄₀]³⁻ Keggin ion as effective electrocatalysts for HER [91]. Spectra and electrochemical results demonstrated that the electroactive sites were the tungstate oxycarbides formed on nanotubes by W-C covalent bonds. Bonchio et al. entrapped {Ru₄SiW₁₀} on multiwall CNTs to obtain high efficient catalyst with low overpotential for OER [92]. Very recently, Li et al. fabricated a cobalt molybdenum phosphide nanocrystal coated by few-layer N-doped carbon shell (donated as CoMoP@C) on a large scale by utilizing {Co₁₆Mo₁₆P₂₄} as precursor [93]. The mixture of {Co₁₆Mo₁₆P₂₄} and dicyandiamide was initially heated at 500°C for 30 min and then heated at 800°C in a flow of ultrapure N₂ atmosphere with different N₂ flow rate to obtain CoMoP@C. It could be used directly in seawater. It exhibited excellent electrocatalytic activity for HER over the whole pH range, which was close to 20% Pt/C in pH = 0–1 media and superior to 20% Pt/C in pH = 2–14 solution. Theoretical investigation demonstrated that the carbon shell acted as a template, prevented the catalyst from agglomeration, and facilitated the porousness and electroconductivity of the catalysts.

GO-based materials are quite intriguing because of their good conductivity, chemically toleration, and large surface area. Such properties suggest wide applications of GO-based materials [94, 95]. More recently, a class of green materials based on the cyclic 48-tungsto-8-phosphate [H₇P₈W₄₈O₁₈₄]³³⁻ and the reduced GO was used for highly active HER electrocatalyst by Zhang and coworkers [96]. P₈W₄₈/rGO was prepared by one-step electrochemical reduction method

(Fig. 15) and it exhibited an exceptionally low overpotential of 28 mV at a current density of 10 mA cm^{-2} , a small Tafel slope of 38 mV dec^{-1} as well as remarkable long-term cycle stability during prolonged potential cycling (Fig. 16). The choice of the macrocyclic POM $\{\text{P}_8\text{W}_{48}\}$ serving as an efficient graphite oxide reductant as precursors was very important [96]. In comparison, a much higher overpotential of 188 mV was obtained for $\text{H}_2\text{W}_{12}/\text{rGO}$ at a current density of 10 mA cm^{-2} . The electrochemical behavior of $\text{P}_8\text{W}_{48}/\text{rGO}$ was comparable well with those of Pt/C, which represented the most convincing experimental examples of the predicted “microenvironment effect.”

Dispersing POMs on specific substrates (e.g., graphene or RGO) could greatly improve the catalyst activities due to the enhancement of conductivity and enlargement of specific surface area of POMs. The above example provided a good synthetic path for synthesizing POM-based GO composites by electrochemical reduction [96]. Then, the question is that how to simply mix POMs and GO without extra voltage? And this is unfortunate, because the interaction between POMs and carbon materials is weak, and thus POMs fall off easily. To solve this problem, conducting organic polymer, ionic liquid, or dye were introduced. Then, Lan et al. prepared a family of hybrid materials consisting of POMs, conducting polymer, and

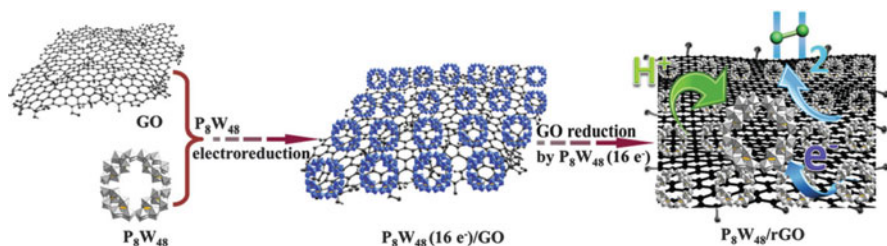


Fig. 15 Schematic view of the one-step electrochemical reduction synthesis of the $\text{P}_8\text{W}_{48}/\text{rGO}$ nanocomposite [96]. Copyright 2016, Royal Society of Chemistry

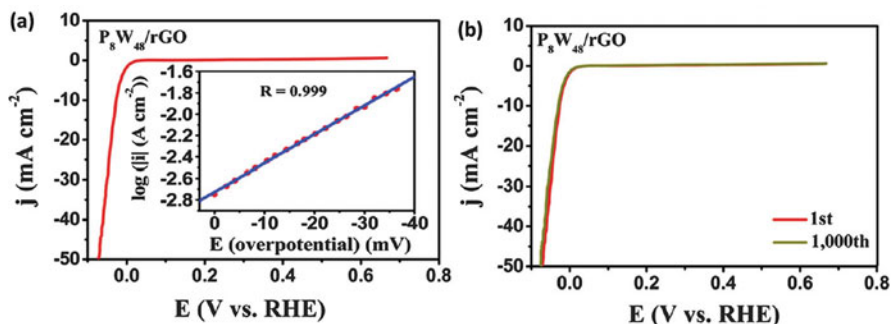


Fig. 16 Electrochemical characterization of the prepared $\text{P}_8\text{W}_{48}/\text{rGO}$: (a) polarization curves of $\text{P}_8\text{W}_{48}/\text{rGO}$, and the *inset* shows the corresponding Tafel plot obtained from the polarization curve, and (b) catalyst stability tests for the composite initially and after 1,000 CV sweeps [96]. Copyright 2016, Royal Society of Chemistry

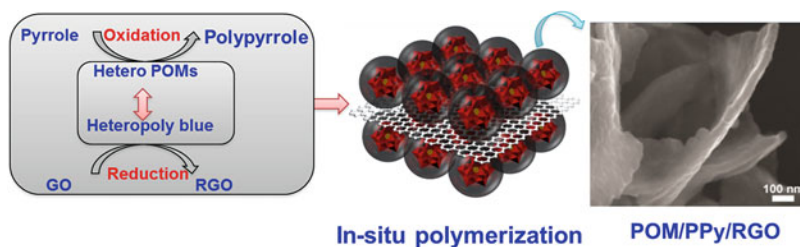


Fig. 17 Synthetic strategy of designing POM/conducting polymer/GO (abbreviated as PCG) substrates (taking conducting polymer of polypyrrole as an example)

RGO substrates (denoted as PCG, Fig. 17) for the following considerations: First, the stacking and aggregation of graphene could be avoided by the introduction of polymer-functionalized POMs. Second, taking pyrrole monomer as an example, it is polymerized into polypyrrole owing to the acidic and oxidative properties of heteropoly acid. Meanwhile the heteropoly acid is reduced to heteropoly blue, and the graphene oxide is reduced to the RGO by the reducing agent-heteropoly blue (Fig. 17). With the polymerization of the pyrrole monomers, POMs are dispersed into the polypyrrole framework. Meanwhile, the RGO is homogeneously distributed and segregated by POMs with wrapped polypyrrole. Third, conducting organic polymers such as polyaniline, polypyrrole, and polythiophene provide C and N sources, and POMs can function as the Mo and P sources, etc. Overall, POMs encapsulated by polypyrrole would be evenly sandwiched between the graphene which is able to be exfoliated to single sheets to form an alternately stacked conformation. This synthetic strategy Lan introduced here not only increases the number of active sites on the materials but also enhances their intrinsic properties such as energy adsorption, electroconductivity, and so on.

Lan's group obtained a ternary POMs-polypyrrole/RGO nanocomposite (POMs-PPy/RGO) by the new synthetic strategy to integrate POMs and pyrrole on graphene sheets via one-pot approach [97]. The homogeneous dispersion of the ternary POMs-PPy/RGO as a precursor was further carbonized at high-reaction temperature, leading to a porous uniform thin layer RGO-supported Mo-based two-dimensional coupled hybrid ($\text{Mo}_2\text{C}@\text{NPC}/\text{NPRGO}$) (Fig. 18). The hybrid consists of Mo_2C encapsulated by N,P-codoped carbon shells and N,P-codoped RGO, exhibiting outstanding electrocatalytic activity for HER with a low onset potential of 0 mV, a low overpotential of 34 mV at a current density of 10 mA cm^{-2} , and a small Tafel slope of 33.6 mV dec^{-1} (Fig. 19). There are three main advantages for these excellent electrocatalysts: (1) the Mo_2C NPs are nanosized and uniformly embedded in the carbon shells without aggregation; (2) the Mo_2C NPs are coated with carbon matrices, which prevent Mo_2C NPs from aggregating or oxidizing and impart them with fast electron transfer ability; and (3) the heteroatom dopants (N, P) provide a large number of exposed active sites. Such efficient catalysts were further verified by theoretical studies, which demonstrated that the reason ascribes to the synergistic effect between

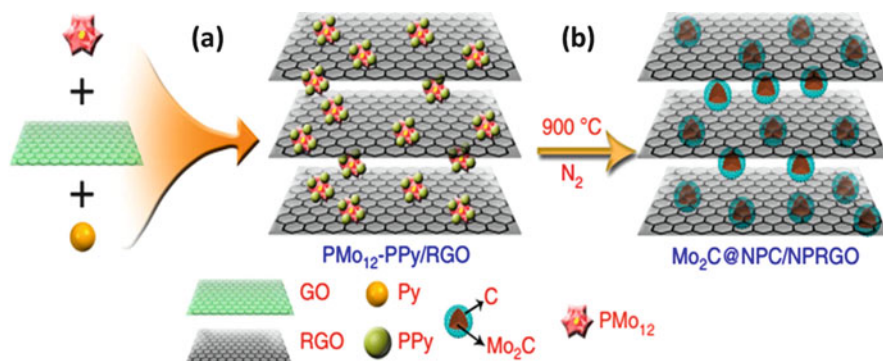


Fig. 18 Schematic construction of $\text{Mo}_2\text{C}@\text{NPC}/\text{NPRGO}$. (a) Synthesis of POMs-PPy/RGO via one-pot reaction. (b) Formation of $\text{Mo}_2\text{C}@\text{NPC}/\text{NPRGO}$ after carbonizing at 900°C in a flow of ultrapure N_2 atmosphere [97]. Copyright 2016, Nature Publishing group

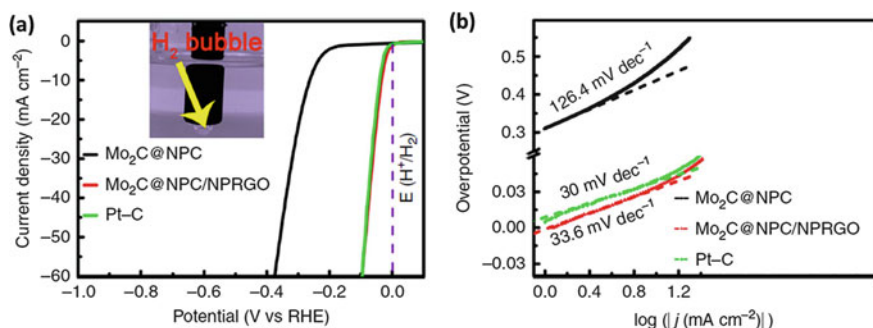
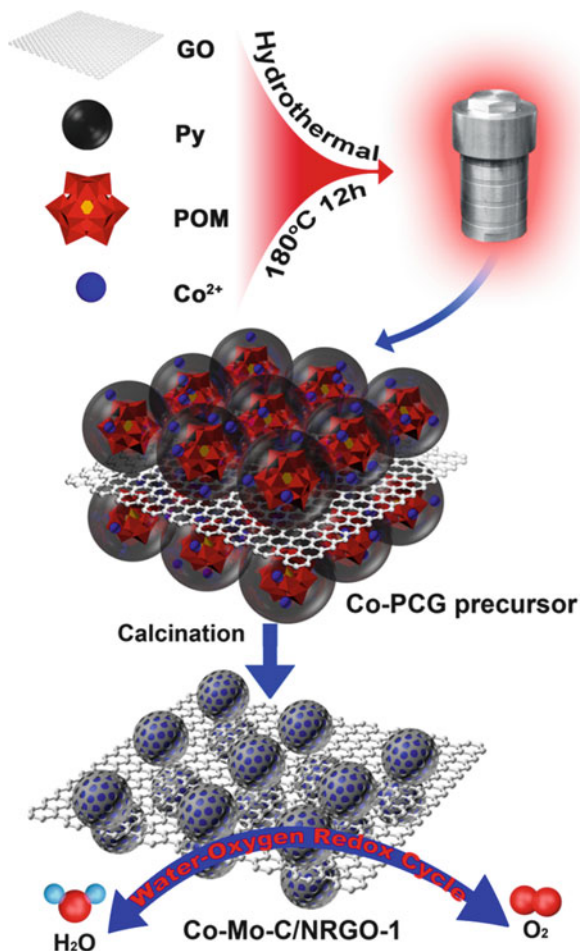


Fig. 19 (a, b) Polarization curves and Tafel plots of the prepared $\text{Mo}_2\text{C}@\text{NPC}/\text{NPRGO}$, and the inset shows the production of H_2 bubbles on the surface of $\text{Mo}_2\text{C}@\text{NPC}/\text{NPRGO}$ [97]. Copyright 2016, Nature Publishing group

Mo_2C and C-pyridinic N. $\text{Mo}_2\text{C}@\text{C}$ -pyridinic N had an appropriate ΔG_{H^*} value for the adsorption and desorption of hydrogen.

The PCG composites, which combined the advantages of conductive polymers and graphene film, can be prepared in large scales through a simple one-pot stirring or hydrothermal method. In addition, introducing the second transition metal to PCG systems (denoted as metal-PCG) not only retains the structure and morphology of PCG but also fine-tunes the structure of carbides together with the bimetallic effect and eventually to enhance simultaneously the electrocatalytic activity for the obtained bimetallic carbide-based materials [98–100]. Recently, Lan et al. have synthesized Co-Mo-C/NRGO-1 by the temperature programmed reduction (TPR) method utilizing the metal-PCG system as precursor (Fig. 20) [101]. The Co-PCG composite was simply prepared by a simple mixture of PMo_{12} , Py, GO films, and $\text{Co}(\text{NO}_3)_2$ using a hydrothermal method, which was further carbonized directly in a horizontal tube furnace at 800°C in a flow of ultrapure N_2 atmosphere. The resulting

Fig. 20 Schematic construction of Co–Mo–C/NRGO-1 composite [101]. Copyright 2016, Nature Publishing group



Co–Mo–C/NRGO-1 composite exhibited surprisingly high OER and ORR performance as a bifunctional electrocatalyst (Fig. 21). The OER performance of Co–Mo–C/NRGO-1 was the best among all the reported carbide-based materials and was comparable to the best OER electrodes with an ultra-low Tafel slope of 42 mV dec^{-1} , a small overpotential of 330 mV vs. RHE at the current density of 10 mA cm^{-2} , and long-term stability in alkaline electrolyte. The ORR performance was also investigated with a positive onset potential ($\sim -95 \text{ mV vs. Ag/AgCl}$), remarkable stability over 30,000 s, and good tolerance to methanol crossover.

POMs are a class of structurally well-defined metal-oxygen (usually composed of MoO_6 , WO_6 , and V_2O_5) anionic clusters. Polyoxomolybdenum as precursors have been studied in PCG systems for HER, for the analogue structure of polyoxomolybdenum which gave impetus to study on the preparation and characterization of polyoxotungstate based composites. In particular, in recent years considerable efforts have been devoted to enhance the activity of tungsten carbides

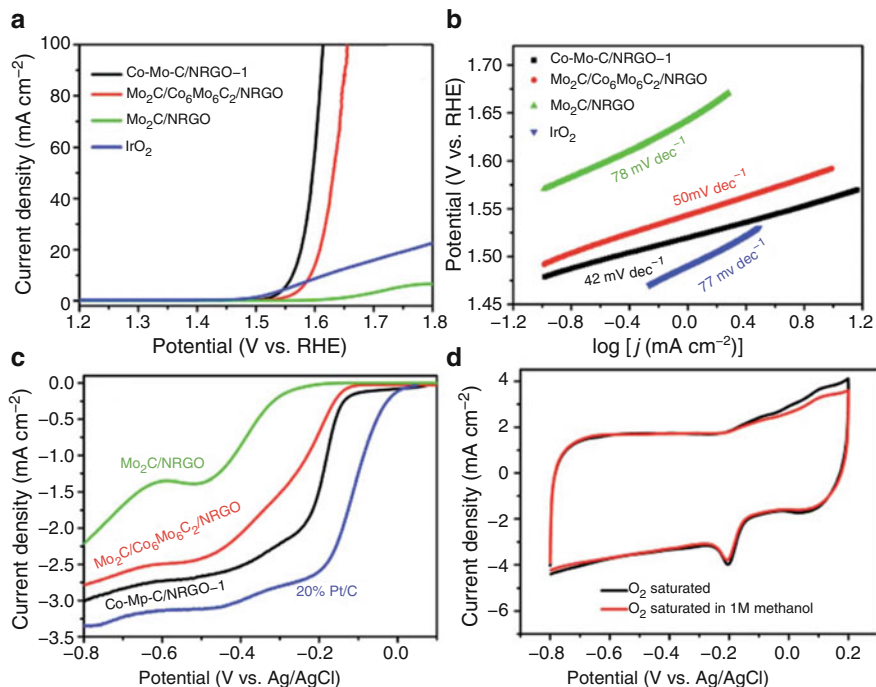


Fig. 21 Electrochemical characterization of the prepared Co-Mo-C/NRGO-1 composite: (a) linear sweep voltammetry (LSV) curves of Co-Mo-C/NRGO-1 composite and the comparable samples with a scan rate of 5 mV s⁻¹ for oxygen evolution reaction (OER). (b) The corresponding Tafel plots derived from (a). (c) LSV curves of Co-Mo-C/NRGO-1 and the comparable samples with a scan rate of 5 mV s⁻¹ and a rotation speed of 1,600 rpm. (d) CV curves of Co-Mo-C/NRGO-1 in 0.1 M KOH without and with 1 M MeOH [101]. Copyright 2016, Royal Society of Chemistry

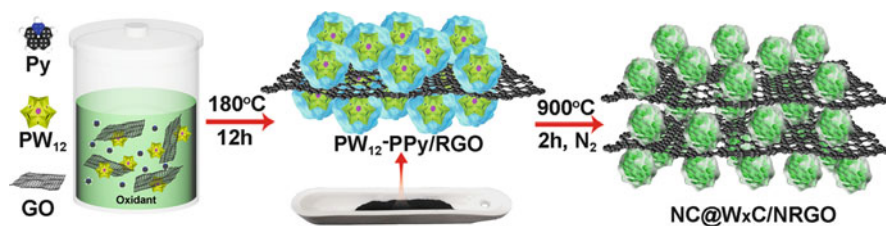


Fig. 22 Schematic construction of NC@W_xC/NRGO composite [106]. Copyright 2017, Wiley

which have been actively studied for its Pt-like behavior [102–105]. Lan et al. have carefully fabricated a two-dimensional coupled hybrid NC@W_xC/NRGO [106] consisting of tungsten carbide (WC, W₂C) encapsulated by N-doped RGO (Fig. 22). First, {PW₁₂}, pyrrole monomer, the assisted oxidant FeCl₃·6H₂O, and graphene oxide were mixed according to the corresponding ratios to synthesize PCG system by one-pot hydrothermal method. Then, the obtained sample was

further carbonized in a horizontal tube furnace at 900°C in a flow of ultrapure N₂ atmosphere. The resulting NC@W_xC/NRGO composite exhibited excellent HER performance in acidic media, with an onset potential of 24 mV and an overpotential of 100 mV at the current density of 10 mA cm⁻², a small Tafel slope of 58.4 mV dec⁻¹ as well as remarkable long-term cycle stability (Fig. 23). This has been one of the highest HER catalysts among the tungsten carbides-based materials ever reported. Very recently, Li et al. reported tungsten carbide NPs encapsulated in N-carbon (donated as P-W₂C@NC) by utilizing PW₁₂ as precursor [107]. The mixture of {PW₁₂} and dicyandiamide was initially heated at 400°C for 30 min and then heated at 800°C in a flow of ultrapure N₂ atmosphere with different N₂ flow rates to obtain the N-carbon coated P-modified tungsten carbide composite, which exhibited excellent electrocatalytic activity for HER over the whole pH range, with a low overpotential of 63 mV in alkaline medium, 89 mV in acid solution, and 185 mV in neutral electrolyte, all at a current density of 10 mA cm⁻².

Beyond the excitement for POM-based metal carbides, metal oxides, the class of transition metal dichalcogenides is of particular interest because of their low economic cost and edge-terminated structure among 2D materials, showing remarkable performance as HER electrocatalysts [108–110]. MoS₂ showing S-Mo-S layers through weak van der Waals interaction has the catalytic active sites, which has been verified by theoretical studies [111–114]. Lan's group devoted efforts to increase the interlayer spacing of MoS₂ and avoid the severe stacking of MoS₂-based materials by introducing small molecules, and further to improve the HER activity. Lan et al. have carefully fabricated a family of uniformly MoS₂/nitrogen-doped RGO nanocomposites MoS₂/N-RGO-*T* consisting of an ultrathin molybdenum disulfide encapsulated by N-doped RGO with interlayer spacing ranging from 6.2 to 9.5 Å (Fig. 24) [108]. First, PMo₁₂ was dissolved in homogeneous GO solution by ultra-sonication for a few minutes. Then, thiourea was added to the above solution and the mixtures with different molar ratios and concentration ratios were heated in a Teflon-lined autoclave by one-pot hydrothermal method. Experimental study showed that when the reaction was heated at 160 or 180°C for

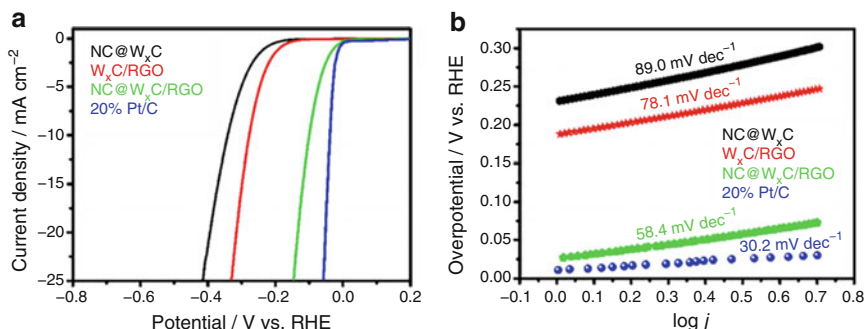


Fig. 23 Electrochemical characterization of the prepared NC@W_xC/NRGO composite: (a) LSV curves of NC@W_xC/NRGO composite and the comparable samples. (b) The corresponding Tafel plots derived from (a) [106]. Copyright 2017, Wiley

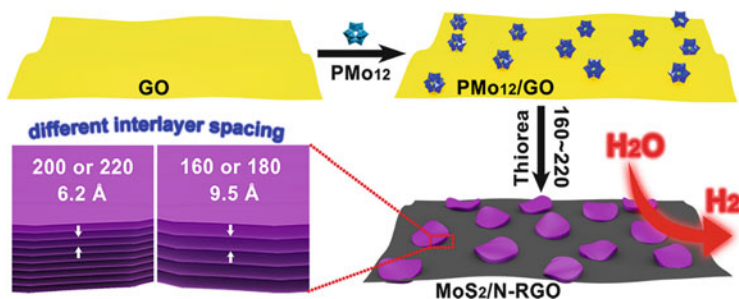


Fig. 24 Schematic constructions of $\text{MoS}_2/\text{N-RGO-T}$ composite [108]. Copyright 2016, Wiley

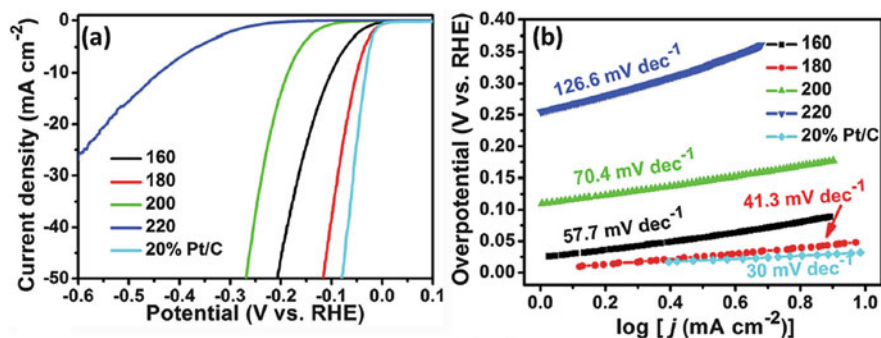


Fig. 25 Electrochemical characterization of the prepared $\text{MoS}_2/\text{N-RGO-T}$ composites: (a) LSV curves of $\text{MoS}_2/\text{N-RGO-T}$ composites at different temperatures; and (b) the corresponding Tafel plots [108]. Copyright 2016, Wiley

24 h, the MoS_2 nanosheet for $\text{MoS}_2/\text{N-RGO}$ had the most enlarged interlayer spacing of 9.5 Å, whereas, the reaction temperature was higher than 180°C, the interlayer spacing decreased to 6.2 Å. The resulting $\text{MoS}_2/\text{N-RGO-180}$ composite exhibited excellent HER performance in acidic media, with an onset potential of −5 mV and an overpotential of 56 mV at the current density of 10 mA cm^{-2} , a small Tafel slope of 41.3 mV dec^{-1} as well as remarkable long-term cycle stability (Fig. 25).

6 Summary and Outlooks

In this chapter, we have presented an overview of progress in POMs, POMOFs, and POM-based materials for electrochemical catalysis applications. The pure POMs have been exploited for catalysis due to their rich electronic properties and high redox activity. However, the design of an ideal electrocatalyst with low-cost, high activity, high porosity, and large number of exposed active sites is quite challenging. The major drawbacks associated with POMs are their high solubility and low

surface area, which have been addressed by either compositing with tunable porous MOFs or coating POMs on highly conductive, porous carbon materials. The developed composites will provide several advantages, for example: (1) the introduction of MOFs or porous substrates will help maintain the porosity for mass transport. (2) The calcination of POMs or POMOFs will lead to formation of highly active sites on the template surface, and thus for stabilizing structure and diffusing mass faster. Such design could be summarized to three steps: (1) Functional orientation selection and synthesis of stable POMs; (2) making POM-based materials; and (3) applying to energy storage and conversion. Due to the multifunctional nature of POMs materials, it is certain that the versatility and generality of this POMs-assisted strategy would continue to expand and the application of such materials would be significantly broadened to other areas, such as lithium battery, lithium-sulfur battery, and so on.

References

1. Turner JA (2004) Sustainable hydrogen production. *Science* 305(5686):972–974
2. Subbaraman R, Tripkovic D, Strmcnik D, Chang K-C, Uchimura M, Paulikas AP, Stamenkovic V, Markovic NM (2011) Enhancing hydrogen evolution activity in water splitting by tailoring $\text{Li}^+\text{-Ni(OH)}_2\text{-Pt}$ interfaces. *Science* 334(6060):1256
3. Subbaraman R, Tripkovic D, Chang K-C, Strmcnik D, Paulikas AP, Hirunsit P, Chan M, Greeley J, Stamenkovic V, Markovic NM (2012) Trends in activity for the water electrolyser reactions on 3d M(Ni,Co,Fe,Mn) hydr(oxy)oxide catalysts. *Nat Mater* 11(6):550–557
4. Lim H-D, Yun YS, Cho SY, Park K-Y, Song MY, Jin H-J, Kang K (2017) All-carbon-based cathode for a true high-energy-density Li-O_2 battery. *Carbon* 114:311–316
5. Lee G-H, Lee S, Kim J-C, Kim DW, Kang Y, Kim D-W (2017) MnMoO_4 electrocatalysts for superior long-life and high-rate lithium-oxygen batteries. *Adv Energy Mater* 7(6):1601741
6. Wu X, Han X, Ma X, Zhang W, Deng Y, Zhong C, Hu W (2017) Morphology-controllable synthesis of Zn-Co -mixed sulfide nanostructures on carbon fiber paper toward efficient rechargeable zinc–air batteries and water electrolysis. *ACS Appl Mater Interfaces* 9(14):12574–12583
7. Cheng Y, Dou S, Veder J-P, Wang S, Saunders M, Jiang SP (2017) Efficient and durable bifunctional oxygen catalysts based on NiFeO@MnOx core–shell structures for rechargeable Zn–Air batteries. *ACS Appl Mater Interfaces* 9(9):8121–8133
8. Lin D, Liu Y, Cui Y (2017) Reviving the lithium metal anode for high-energy batteries. *Nat Nanotechnol* 12(3):194–206
9. Walter MG, Warren EL, McKone JR, Boettcher SW, Mi Q, Santori EA, Lewis NS (2010) Solar water splitting cells. *Chem Rev* 110(11):6446–6473
10. Wang J, Yang J-Y, Fazal IM, Ahmed N, Yan Y, Huang H, Ren Y, Yue Y, Dolinar S, Tur M, Willner AE (2012) Terabit free-space data transmission employing orbital angular momentum multiplexing. *Nat Photonics* 6(7):488–496
11. Reece SY, Hamel JA, Sung K, Jarvi TD, Esswein AJ, Pijpers JJH, Nocera DG (2011) Wireless solar water splitting using silicon-based semiconductors and earth-abundant catalysts. *Science* 334(6056):645
12. Carmo M, Fritz DL, Mergel J, Stolten D (2013) A comprehensive review on PEM water electrolysis. *Int J Hydrogen Energy* 38(12):4901–4934
13. Peighambaroust SJ, Rowshanzamir S, Amjadi M (2010) Review of the proton exchange membranes for fuel cell applications. *Int J Hydrogen Energy* 35(17):9349–9384

14. Zeng K, Zhang D (2010) Recent progress in alkaline water electrolysis for hydrogen production and applications. *Prog Energy Combust Sci* 36(3):307–326
15. Barbir F (2005) PEM electrolysis for production of hydrogen from renewable energy sources. *Sol Energy* 78(5):661–669
16. Liang Y, Li Y, Wang H, Dai H (2013) Strongly coupled inorganic/nanocarbon hybrid materials for advanced electrocatalysis. *J Am Chem Soc* 135(6):2013–2036
17. Vrubel H, Hu X (2012) Molybdenum boride and carbide catalyze hydrogen evolution in both acidic and basic solutions. *Angew Chem Int Ed* 51(51):12703–12706
18. Song J, Li GR, Xiong FY, Gao XP (2012) Synergistic effect of molybdenum nitride and carbon nanotubes on electrocatalysis for dye-sensitized solar cells. *J Mater Chem* 22(38):20580–20585
19. Weidman MC, Esposito DV, Hsu Y-C, Chen JG (2012) Comparison of electrochemical stability of transition metal carbides (WC, W₂C, Mo₂C) over a wide pH range. *J Power Sources* 202:11–17
20. Wan C, Regmi YN, Leonard BM (2014) Multiple phases of molybdenum carbide as electrocatalysts for the hydrogen evolution reaction. *Angew Chem Int Ed* 53(25):6407–6410
21. Dong S, Chen X, Zhang X, Cui G (2013) Nanostructured transition metal nitrides for energy storage and fuel cells. *Coord Chem Rev* 257(13–14):1946–1956
22. Hargreaves JSJ (2013) Heterogeneous catalysis with metal nitrides. *Coord Chem Rev* 257(13–14):2015–2031
23. Chen W-F, Sasaki K, Ma C, Frenkel AI, Marinkovic N, Muckerman JT, Zhu Y, Adzic RR (2012) Hydrogen-evolution catalysts based on non-noble metal nickel–molybdenum nitride nanosheets. *Angew Chem Int Ed* 51(25):6131–6135
24. Cao B, Veith GM, Neufeind JC, Adzic RR, Khalifah PG (2013) Mixed close-packed cobalt molybdenum nitrides as non-noble metal electrocatalysts for the hydrogen evolution reaction. *J Am Chem Soc* 135(51):19186–19192
25. Zhang X, Zhang Q, Sun Y, Zhang P, Gao X, Zhang W, Guo J (2016) MoS₂-graphene hybrid nanosheets constructed 3D architectures with improved electrochemical performance for lithium-ion batteries and hydrogen evolution. *Electrochim Acta* 189:224–230
26. Ganesan R, Lee JS (2005) Tungsten carbide microspheres as a noble-metal-economic electrocatalyst for methanol oxidation. *Angew Chem Int Ed* 44(40):6557–6560
27. Zhang Y, Zhang Y, Ji Q, Ju J, Yuan H, Shi J, Gao T, Ma D, Liu M, Chen Y (2013) Controlled growth of high-quality monolayer WS₂ layers on sapphire and imaging its grain boundary. *ACS Nano* 7(10):8963–8971
28. Voiry D, Yamaguchi H, Li J, Silva R, Alves DCB, Fujita T, Chen M, Asefa T, Shenoy VB, Eda G, Chhowalla M (2013) Enhanced catalytic activity in strained chemically exfoliated WS₂ nanosheets for hydrogen evolution. *Nat Mater* 12(9):850–855
29. Yang J, Voiry D, Ahn SJ, Kang D, Kim AY, Chhowalla M, Shin HS (2013) Two-dimensional hybrid nanosheets of tungsten disulfide and reduced graphene oxide as catalysts for enhanced hydrogen evolution. *Angew Chem Int Ed* 52(51):13751–13754
30. Peng S, Li L, Han X, Sun W, Srinivasan M, Mhaisalkar SG, Cheng F, Yan Q, Chen J, Ramakrishna S (2014) Cobalt sulfide nanosheet/graphene/carbon nanotube nanocomposites as flexible electrodes for hydrogen evolution. *Angew Chem Int Ed* 126(46):12802–12807
31. Jiang P, Liu Q, Liang Y, Tian J, Asiri AM, Sun X (2014) A cost-effective 3D hydrogen evolution cathode with high catalytic activity: FeP nanowire array as the active phase. *Angew Chem Int Ed* 53(47):12855–12859
32. Popczun EJ, McKone JR, Read CG, Biacchi AJ, Wiltout AM, Lewis NS, Schaak RE (2013) Nanostructured nickel phosphide as an electrocatalyst for the hydrogen evolution reaction. *J Am Chem Soc* 135(25):9267–9270
33. Pu Z, Liu Q, Tang C, Asiri AM, Sun X (2014) Ni₂P nanoparticle films supported on a Ti plate as an efficient hydrogen evolution cathode. *Nanoscale* 6(19):11031–11034

34. Huang Z, Chen Z, Chen Z, Lv C, Meng H, Zhang C (2014) Ni_{12}P_5 nanoparticles as an efficient catalyst for hydrogen generation via electrolysis and photoelectrolysis. *ACS Nano* 8 (8):8121–8129
35. Jiang P, Liu Q, Sun X (2014) NiP_2 nanosheet arrays supported on carbon cloth: an efficient 3D hydrogen evolution cathode in both acidic and alkaline solutions. *Nanoscale* 6(22):13440
36. Zhan T, Liu X, Lu S, Hou W (2017) Nitrogen doped NiFe layered double hydroxide/reduced graphene oxide mesoporous nanosphere as an effective bifunctional electrocatalyst for oxygen reduction and evolution reactions. *Appl Catal B* 205:551–558
37. Jia Y, Zhang L, Gao G, Chen H, Wang B, Zhou J, Soo MT, Hong M, Yan X, Qian G (2017) A heterostructure coupling of exfoliated Ni-Fe hydroxide nanosheet and defective graphene as a bifunctional electrocatalyst for overall water splitting. *Adv Mater* 29:1700017
38. Weng B, Xu F, Wang C, Meng W, Grice CR, Yan Y (2016) A layered $\text{Na}_{1-x}\text{Ni}_y\text{Fe}_{1-y}\text{O}_2$ double oxide oxygen evolution reaction electrocatalyst for highly efficient water-splitting. *Energy Environ Sci* 10:121–128
39. Candelaria SL, Bedford NM, Woehl TJ, Rentz NS, Showalter AR, Pylypenko S, Bunker BA, Lee S, Reinhart B, Ren Y, Ertem SP, Coughlin EB, Sather NA, Horan JL, Herring AM, Greenlee LF (2017) Multi-component Fe-Ni hydroxide nanocatalyst for oxygen evolution and methanol oxidation reactions under alkaline conditions. *ACS Catal* 7(1):365–379
40. Zheng Y, Jiao Y, Li LH, Xing T, Chen Y, Jaroniec M, Qiao SZ (2014) Toward design of synergistically active carbon-based catalysts for electrocatalytic hydrogen evolution. *ACS Nano* 8(5):5290–5296
41. Gao S, Li GD, Liu Y, Chen H, Feng LL, Wang Y, Yang M, Wang D, Wang S, Zou X (2014) Electrocatalytic H_2 production from seawater over Co, N-codoped nanocarbons. *Nanoscale* 7 (6):2306
42. Zou X, Huang X, Goswami A, Silva R, Sathe BR, Mikmeková E, Asefa T (2014) Cobalt-embedded nitrogen-rich carbon nanotubes efficiently catalyze hydrogen evolution reaction at all pH values. *Angew Chem Int Ed* 53(17):4372–4376
43. Deng J, Ren P, Deng D, Yu L, Yang F, Bao X (2014) Highly active and durable non-precious-metal catalysts encapsulated in carbon nanotubes for hydrogen evolution reaction. *Energy Environ Sci* 7(6):1919–1923
44. Zou X, Zhang Y (2015) Noble metal-free hydrogen evolution catalysts for water splitting. *Chem Soc Rev* 44(15):5148–5180
45. Cook TR, Dogutan DK, Reece SY, Surendranath Y, Teets TS, Nocera DG (2010) Solar energy supply and storage for the legacy and nonlegacy worlds. *Chem Rev* 110 (11):6474–6502
46. Mizuno N, Misono M (1998) Heterogeneous catalysis. *Chem Rev* 98(1):199–218
47. Pope MT, Müller A (1991) Polyoxometalate chemistry: an old field with new dimensions in several disciplines. *Angew Chem Int Ed Engl* 30(1):34–48
48. Naruke H, Yamase T (1992) Structure of a photoluminescent polyoxotungstoantimonate. *Acta Cryst Sect C* 48(4):597–599
49. Schmidt KJ, Schrobilgen GJ, Sawyer JF (1986) Hexasodium hexatungstotellurate(VI) 22-hydrate. *Acta Cryst Sect C* 42(9):1115–1118
50. Nolan AL, Burns RC, Lawrance GA, Craig DC (2000) Octasodium hexatungstomanganate (IV) octadecahydrate. *Acta Cryst Sect C* 56(7):729–730
51. Pope MT (1983) Heteropoly and isopoly oxometalates. Springer, Berlin
52. Dawson B (1953) The structure of the 9(18)-heteropoly anion in potassium 9(18)-tungstophosphate, $\text{K}_6(\text{P}_2\text{W}_{18}\text{O}_{62}) \cdot 14\text{H}_2\text{O}$. *Acta Crystallogr* 6(2):113–126
53. Müller A, Krickemeyer E, Bögge H, Schmidtmann M, Peters F (1998) Organizational forms of matter: an inorganic super fullerene and keplerate based on molybdenum oxide. *Angew Chem Int Ed* 37(24):3359–3363
54. Wang H, Hamanaka S, Nishimoto Y, Irle S, Yokoyama T, Yoshikawa H, Awaga K (2012) In operando X-ray absorption fine structure studies of polyoxometalate molecular cluster batteries: polyoxometalates as electron sponges. *J Am Chem Soc* 134(10):4918–4924

55. Keita B, Nadjo L (2006) In: Bard AJ, Stratmann M (eds) *Encyclopedia of electrochemistry*, vol 7. Wiley-VCH, Weinheim
56. Keita B, Kortz U, Holze LRB, Brown S, Nadjo L (2007) Efficient hydrogen-evolving cathodes based on proton and electron reservoir behaviors of the phosphotungstate $[\text{H}_7\text{P}_8\text{W}_{48}\text{O}_{184}]^{33-}$ and the Co(II)-containing silicotungstates $[\text{Co}_6(\text{H}_2\text{O})_{30}\{\text{Co}_9\text{Cl}_2(\text{OH})_3(\text{H}_2\text{O})_9(\beta\text{-SiW}_8\text{O}_{31})_3\}]^{5-}$ and $[\{\text{Co}_3(\text{B-}\beta\text{-SiW}_9\text{O}_{33}(\text{OH}))(\text{B-}\beta\text{-SiW}_8\text{O}_{29}(\text{OH})_2)\}_2]^{22-}$. *Langmuir* 23(19):9531–9534
57. Keita B, Lu YW, Nadjo L, Contant R (2000) Salient electrochemical and electrocatalytic behaviour of the crown heteropolyanion $\text{K}_{28}\text{Li}_5\text{H}_7\text{P}_8\text{W}_{48}\text{O}_{184}\cdot 92\text{H}_2\text{O}$. *Electrochem Commun* 2(10):720–726
58. Banerjee A, Bassil BS, Roschenthaler G-V, Kortz U (2012) Diphosphates and diphosphonates in polyoxometalate chemistry. *Chem Soc Rev* 41(22):7590–7604
59. Prabhakaran V, Mehdi BL, Ditto JJ, Engelhard MH, Wang B, Gunaratne KDD, Johnson DC, Browning ND, Johnson GE, Laskin J (2016) Rational design of efficient electrode–electrolyte interfaces for solid-state energy storage using ion soft landing. *Nat Commun* 7:11399
60. Barras-Almenar JJ, Coronado E, Müller A, Pope MT (2003) Polyoxometalate molecular science, vol 35. Springer, Dordrecht
61. Dolbecq A, Mialane P, Secheresse F, Keita B, Nadjo L (2012) Functionalized polyoxometalates with covalently linked bisphosphonate, N-donor or carboxylate ligands: from electrocatalytic to optical properties. *Chem Commun* 48(67):8299–8316
62. Rhule JT, Hill CL, Judd DA, Schinazi RF (1998) Polyoxometalates in medicine. *Chem Rev* 98(1):327–358
63. Nomiya K, Torii H, Hasegawa T, Nemoto Y, Nomura K, Hashino K, Uchida M, Kato Y, Shimizu K, Oda M (2001) Insulin mimetic effect of a tungstate cluster. Effect of oral administration of homo-polyoxotungstates and vanadium-substituted polyoxotungstates on blood glucose level of STZ mice. *J Inorg Biochem* 86(4):657–667
64. Yamase T (2005) Anti-tumor, -viral, and -bacterial activities of polyoxometalates for realizing an inorganic drug. *J Mater Chem* 15(45):4773–4782
65. Vasylyev MV, Neumann R (2003) New heterogeneous polyoxometalate based mesoporous catalysts for hydrogen peroxide mediated oxidation reactions. *J Am Chem Soc* 126(3):884–890
66. Mbomekalle IM, Keita B, Nadjo L, Berthet P, Hardcastle KI, Hill CL, Anderson TM (2003) Multi-iron tungstodiarisenes. Synthesis, characterization, and electrocatalytic studies of $\alpha\beta\alpha\text{-(Fe}^{\text{III}}\text{OH}_2)_2\text{Fe}^{\text{III}}(\text{As}_2\text{W}_{15}\text{O}_{56})_2^{12-}$. *Inorg Chem* 42(4):1163–1169
67. Sartorel A, Bonchio M, Campagna S, Scandola F (2013) Tetrametallic molecular catalysts for photochemical water oxidation. *Chem Soc Rev* 42(6):2262–2280
68. Berardi S, La Ganga G, Natali M, Bazzan I, Puntoriero F, Sartorel A, Scandola F, Campagna S, Bonchio M (2012) Photocatalytic water oxidation: tuning light-induced electron transfer by molecular Co_4O_4 cores. *J Am Chem Soc* 134(27):11104–11107
69. Hill CL, Gueletii YV, Musaev DG, Yin Q, Botar B (2012) Polyoxometalate water oxidation catalysts and methods of use thereof. US20120027666A1
70. Miras HN, Yan J, Long DL, Cronin L (2012) Engineering polyoxometalates with emergent properties. *Chem Soc Rev* 41(22):7403–7430
71. Long DL, Burkholder E, Cronin L (2007) Polyoxometalate clusters, nanostructures and materials: from self assembly to designer materials and devices. *Chem Soc Rev* 36(1):105–121
72. Nyman M (2011) Polyoxoniobate chemistry in the 21st century. *Dalton Trans* 40(32):8049–8058
73. Song YF, Tsunashima R (2012) Recent advances on polyoxometalate-based molecular and composite materials. *Chem Soc Rev* 41(22):7384–7402
74. Conway BE, Bai L, Sattar MA (1987) Role of the transfer coefficient in electrocatalysis: applications to the H_2 and O_2 evolution reactions and the characterization of participating adsorbed intermediates. *Int J Hydrogen Energy* 12(9):607–621

75. Rausch B, Symes MD, Chisholm G, Cronin L (2014) Decoupled catalytic hydrogen evolution from a molecular metal oxide redox mediator in water splitting. *Science* 345(6202):1326
76. Keita B, Nadjo L (2007) Electrochemical reactions on modified electrodes. In: Bard AJ, Stratmann M (eds) *Encyclopedia of electrochemistry*, vol 11. Wiley-VCH, Weinheim, pp 685–728
77. Du D-Y, Qin J-S, Li S-L, Su Z-M, Lan Y-Q (2014) Recent advances in porous polyoxometalate-based metal-organic framework materials. *Chem Soc Rev* 43(13):4615–4632
78. Striegler K, Glaeser R (2016) Strategies towards improved efficiency in photocatalytic hydrogen evolution from aqueous media. *Prepr Am Chem Soc Div Energy Fuels* 61(1):214–215
79. Schoenweiz S, Rommel SA, Kuebel J, Micheel M, Dietzek B, Rau S, Streb C (2016) Covalent photosensitizer-polyoxometalate-catalyst dyads for visible-light-driven hydrogen evolution. *Chem Eur J* 22(34):12002–12005
80. Nohra B, El Moll H, Rodriguez Albelo LM, Mialane P, Marrot J, Mellot-Draznieks C, O’Keeffe M, Ngo Biboum R, Lemaire J, Keita B, Nadjo L, Dolbecq A (2011) Polyoxometalate-based metal organic frameworks (POMOFs): structural trends, energetics, and high electrocatalytic efficiency for hydrogen evolution reaction. *J Am Chem Soc* 133(34):13363–13374
81. Qin J-S, Du D-Y, Guan W, Bo X-J, Li Y-F, Guo L-P, Su Z-M, Wang Y-Y, Lan Y-Q, Zhou H-C (2015) Ultrastable polymolybdate-based metal-organic frameworks as highly active electrocatalysts for hydrogen generation from water. *J Am Chem Soc* 137(22):7169–7177
82. Wu HB, Xia BY, Yu L, Yu X-Y, Lou XWD (2015) Porous molybdenum carbide nano-octahedrons synthesized via confined carburization in metal-organic frameworks for efficient hydrogen production. *Nat Commun* 6:6512
83. Li J-S, Tang Y-J, Liu C-H, Li S-L, Li R-H, Dong L-Z, Dai Z-H, Bao J-C, Lan Y-Q (2016) Polyoxometalate-based metal-organic framework-derived hybrid electrocatalysts for highly efficient hydrogen evolution reaction. *J Mater Chem A* 4(4):1202–1207
84. Tang Y-J, Gao M-R, Liu C-H, Li S-L, Jiang H-L, Lan Y-Q, Han M, Yu S-H (2015) Porous molybdenum-based hybrid catalysts for highly efficient hydrogen evolution. *Angew Chem Int Ed* 54(44):12928–12932
85. Li J-S, Li S-L, Tang Y-J, Han M, Dai Z-H, Bao J-C, Lan Y-Q (2015) Nitrogen-doped Fe/Fe₃C@graphitic layer/carbon nanotube hybrids derived from MOFs: efficient bifunctional electrocatalysts for ORR and OER. *Chem Commun* 51(13):2710–2713
86. Yang X, Feng X, Tan H, Zang H, Wang X, Wang Y, Wang E, Li Y (2016) N-doped graphene-coated molybdenum carbide nanoparticles as highly efficient electrocatalysts for the hydrogen evolution reaction. *J Mater Chem A* 4(10):3947–3954
87. Barsukova-Stuckart M, Izarova NV, Jameson GB, Ramachandran V, Wang Z, van Tol J, Dalal NS, Ngo Biboum R, Keita B, Nadjo L, Kortz U (2011) Synthesis and characterization of the dicopper(II)-containing 22-palladate(II)[Cu^{II}2Pd^{II}22P^V12O₆₀(OH)₈]²⁰⁻. *Angew Chem Int Ed* 50(11):2639–2642
88. Rousseau G, Zhang S, Oms O, Dolbecq A, Marrot J, Liu R, Shang X, Zhang G, Keita B, Mialane P (2015) Sequential synthesis of 3 d-3 d, 3 d-4 d, and 3 d-5 d hybrid polyoxometalates and application to the electrocatalytic oxygen reduction reaction. *Chem Eur J* 21(34):12153–12160
89. Liu G, Pan J, Yin L, Irvine JTS, Li F, Tan J, Wormald P, Cheng H-M (2012) Heteroatom-modulated switching of photocatalytic hydrogen and oxygen evolution preferences of anatase TiO₂ microspheres. *Adv Funct Mater* 22(15):3233–3238
90. Zhong X, Sun Y, Chen X, Zhuang G, Li X, Wang J-G (2016) Mo doping induced more active sites in urchin-like W₁₈O₄₉ nanostructure with remarkably enhanced performance for hydrogen evolution reaction. *Adv Funct Mater* 26(32):5778–5786
91. Xu W, Liu C, Xing W, Lu T (2007) A novel hybrid based on carbon nanotubes and heteropolyanions as effective catalyst for hydrogen evolution. *Electrochem Commun* 9(1):180–184

92. Toma FM, Sartorel A, Iurlo M, Carraro M, Parisse P, Maccato C, Rapino S, Gonzalez BR, Amenitsch H, Da Ros T, Casalis L, Goldoni A, Marcaccio M, Scorrano G, Scoles G, Paolucci F, Prato M, Bonchio M (2010) Efficient water oxidation at carbon nanotube–polyoxometalate electrocatalytic interfaces. *Nat Chem* 2(10):826–831
93. Ma Y-Y, Wu C-X, Feng X-J, Tan H-Q, Yan L-K, Liu Y, Kang Z-H, Wang E-B, Li Y-G (2017) Highly efficient hydrogen evolution from seawater by a low-cost and stable CoMoP@C electrocatalyst superior to Pt/C. *Energy Environ Sci* 10(3):788–798
94. Wang H, Maiyalagan T, Wang X (2012) Review on recent progress in nitrogen-doped graphene: synthesis, characterization, and its potential applications. *ACS Catal* 2(5):781–794
95. Lin Z, Waller GH, Liu Y, Liu M, Wong C-P (2013) Simple preparation of nanoporous few-layer nitrogen-doped graphene for use as an efficient electrocatalyst for oxygen reduction and oxygen evolution reactions. *Carbon* 53:130–136
96. Liu R, Zhang G, Cao H, Zhang S, Xie Y, Haider A, Kortz U, Chen B, Dalal NS, Zhao Y, Zhi L, Wu C-X, Yan L-K, Su Z, Keita B (2016) Enhanced proton and electron reservoir abilities of polyoxometalate grafted on graphene for high-performance hydrogen evolution. *Energy Environ Sci* 9(3):1012–1023
97. Li J-S, Wang Y, Liu C-H, Li S-L, Wang Y-G, Dong L-Z, Dai Z-H, Li Y-F, Lan Y-Q (2016) Coupled molybdenum carbide and reduced graphene oxide electrocatalysts for efficient hydrogen evolution. *Nat Commun* 7:11204
98. Ma X, Meng H, Cai M, Shen PK (2012) Bimetallic carbide nanocomposite enhanced Pt catalyst with high activity and stability for the oxygen reduction reaction. *J Am Chem Soc* 134(4):1954–1957
99. Liu Y, Li G-D, Yuan L, Ge L, Ding H, Wang D, Zou X (2015) Carbon-protected bimetallic carbide nanoparticles for a highly efficient alkaline hydrogen evolution reaction. *Nanoscale* 7(7):3130–3136
100. Xiao P, Ge X, Wang H, Liu Z, Fisher A, Wang X (2015) Novel molybdenum carbide–tungsten carbide composite nanowires and their electrochemical activation for efficient and stable hydrogen evolution. *Adv Funct Mater* 25(10):1520–1526
101. Liu C-H, Tang Y-J, Wang X-L, Huang W, Li S-L, Dong L-Z, Lan Y-Q (2016) Highly active Co-Mo-C/NRGO composite as efficient oxygen electrode for water-oxygen redox cycle. *J Mater Chem A* 4:18100–18106
102. Fan X, Zhou H, Guo X (2015) WC nanocrystals grown on vertically aligned carbon nanotubes: an efficient and stable electrocatalyst for hydrogen evolution reaction. *ACS Nano* 9(5):5125–5134
103. Hunt ST, Nimmanwudipong T, Román-Leshkov Y (2014) Engineering non-sintered, metal-terminated tungsten carbide nanoparticles for catalysis. *Angew Chem Int Ed* 53(20):5131–5136
104. Zhao Y, Kamiya K, Hashimoto K, Nakanishi S (2013) Hydrogen evolution by tungsten carbonitride nanoelectrocatalysts synthesized by the formation of a tungsten acid/polymer hybrid in situ. *Angew Chem Int Ed* 52(51):13638–13641
105. Levy RB, Boudart M (1973) Platinum-like behavior of tungsten carbide in surface catalysis. *Science* 181(4099):547–549
106. Wang X-L, Tang Y-J, Huang W, Liu C-H, Dong L-Z, Li S-L, Lan Y-Q (2017) Efficient electrocatalyst for the hydrogen evolution reaction derived from polyoxotungstate/polypyrrole/graphene. *ChemSusChem* 10:2402–2407
107. Yan G, Wu C, Tan H, Feng X, Yan L, Zang H, Li Y (2016) N-Carbon coated P-W2C composite as efficient electrocatalyst for hydrogen evolution reactions over the whole pH range. *J Mater Chem A* 5:765–772
108. Tang Y-J, Wang Y, Wang X-L, Li S-L, Huang W, Dong L-Z, Liu C-H, Li Y-F, Lan Y-Q (2016) Molybdenum disulfide/nitrogen-doped reduced graphene oxide nanocomposite with enlarged interlayer spacing for electrocatalytic hydrogen evolution. *Adv Energy Mater* 6(12):1600116

109. Morales-Guio CG, Hu X (2014) Amorphous molybdenum sulfides as hydrogen evolution catalysts. *Acc Chem Res* 47(8):2671–2681
110. Tan C, Zhang H (2015) Epitaxial growth of hetero-nanostructures based on ultrathin two-dimensional nanosheets. *J Am Chem Soc* 137(38):12162–12174
111. Jaramillo TF, Jørgensen KP, Bonde J, Nielsen JH, Hørch S, Chorkendorff I (2007) Identification of active edge sites for electrochemical H₂ evolution from MoS₂ nanocatalysts. *Science* 317(5834):100–102
112. Voiry D, Salehi M, Silva R, Fujita T, Chen M, Asefa T, Shenoy VB, Eda G, Chhowalla M (2013) Conducting MoS₂ nanosheets as catalysts for hydrogen evolution reaction. *Nano Lett* 13(12):6222–6227
113. Liao L, Zhu J, Bian X, Zhu L, Scanlon MD, Girault HH, Liu B (2013) MoS₂ formed on mesoporous graphene as a highly active catalyst for hydrogen evolution. *Adv Funct Mater* 23(42):5326–5333
114. Gao M-R, Chan MKY, Sun Y (2015) Edge-terminated molybdenum disulfide with a 9.4-Å interlayer spacing for electrochemical hydrogen production. *Nat Commun* 6:7493